Coherence transfer in two-pulse double quantum (DQ) and five-pulse double- quantum modulation (DQM) sequences in EPR: Orientation selectivity, structural sensitivity and distance measurements

Sushil K. Misra (sushil.misra@concordia.ca)
Concordia University https://orcid.org/0000-0003-2531-3014
Hamid Reza Salahi
Concordia University

Research Article

Keywords: Biological Systems, Nitroxide biradicals, Numerical Algorithms, Finite Pulse, Non-zero Coherence Transfers, Pake Doublets

Posted Date: March 4th, 2021

DOI: https://doi.org/10.21203/rs.3.rs-291882/v1

Coherence transfer in two-pulse double quantum (DQ) and five-pulse double- quantum modulation (DQM) sequences in EPR: Orientation selectivity, structural sensitivity and distance measurements

Sushil K. Misra* and Hamid Reza Salahi
Physics Department, Concordia University,
7141 Sherbrooke St. West, Montreal, QC H4B 1R6, Canada

Abstract. Double-quantum (DQ) coherence transfers in two-pulse DQ and five-pulse DQM (double quantum modulation) EPR pulse sequences, utilized for orientation selectivity and distance measurements in biological systems using nitroxide biradicals, are investigated. Analytical expressions, along with numerical algorithms, for EPR signals are given in full details. It is shown, in general, that a finite pulse, as opposed to an infinite pulse, in conjunction with dipolar interaction between the two nitroxide radicals, is needed to produce non-zero coherence transfers in 0→2 and 2→-1 transitions. Furthermore, the simulations show that the coherence transfer, $T_{0\to2}$, as effected by a finite pulse, increases as the amplitude of the irradiation field (B_1) decreases, being maximum for those coupled nitroxides, whose dipolar axis, i.e., the line joining their dipoles, relative to the external magnetic field, are oriented symmetrically at $\pm 10^{\circ}$ away from the magic angle $\theta_0 \sim 54.74^{\circ}$, at which $(3cos^2\theta - 1) = 0$, and its supplementary angle 125.26°. (Here θ is the angle between the dipolar axis and the external magnetic field,) ***This is a new result, as far as orientational sensitivity of the forbidden DQ signal is concerned, found here with the help of extensive simulations for the first time.*** In addition, it is shown that only measurements involving single time variable are needed to obtain the Pake doublets in polycrystalline (powder) samples to determine the dipolar constant, proportional to the inverse cube of the distance between the nitroxide radicals. The analytical expressions, derived here for the various signals for any fixed orientations of the two nitroxide dipoles with respect to the dipolar axis, show that, in general, the Fourier transforms of the two-pulse DQ sequence exhibit peaks at $\pm\frac{3}{2}d \times (3cos^2\theta - 1)$, whereas the five-pulse DQM sequence exhibits peaks at $\pm d \times (3cos^2\theta - 1)$; where $d = \frac{2}{3}D$, with D being the dipolar-coupling constant. Furthermore, it is found that the signals from two-pulse DQ and five-pulse DQM sequences are sensitive to the orientations of the two nitroxide dipoles, described

by the Euler angles $(\alpha_1, \beta_1, \gamma_1)$; $(\alpha_2, \beta_2, \gamma_2)$. This provides structural sensitivity to the two-pulse DQ and five-pulse DQM signals, useful for understanding the details of the configuration of biomolecules. As for the numerically calculated polycrystalline (powder) averages, accumulated over 20 sets of Monte-Carlo orientations of the two nitroxide dipole moments, it is found that the Pake doublets occur at $\pm\frac{3}{2}d$ for the two-pulse DQ sequence and at $\pm d$ for the five-pulse DQM sequence. The magnitudes of coherence transfers in the transitions 0→2 and 2→-1 are found to be about the same for DQ and DQM sequences, depending on the amplitude of the irradiation field, as well as on the duration of the pulse. They increase significantly with increasing strength of the dipolar constant, d, as calculated here for $d = 10\ and\ 30$ MHz, corresponding to the value of $r =$ 17 and 11 Å. The effect of relaxation in polycrystalline samples is considered by the use of a stretched exponential. The numerical algorithm for the five-pulse DQM sequence presented here is exploited to calculate the intensity of the five-pulse DQM signal to fit the published experimental data; a good agreement is found within the experimental error.

P. A. C. S. Classification: 76.30.-v, 76.70.Dx

* corresponding author; email: sushil.misra@concordia.ca

1. Introduction

It is important to study coherence transfer from one coherent state, $p = 0$, described by the difference in magnetic quantum numbers $p = \Delta M_{rs}$, corresponding to the matrix element ρ_{rs} of the density matrix, to the forbidden one, $p = +2$, which is two quantum numbers different, in pulsed-EPR (Electron Paramagnetic Resonance) experiments [1]. This coherence transfer is known as double quantum (DQ) coherence and has been investigated frequently in NMR (nuclear magnetic resonance) [2-4]. However, unless $p = -1$, it does not lead to observable magnetization. It can, on the other hand, be observed indirectly by transferring the $p = +2$ coherence to $p = -1$ coherence state by a subsequent coherence transfer, similar to that done in NMR [5,6].

The advantage of DQ coherence, is that it depends on the dipolar interaction, so that the intensity of the signal decreases rather slowly with distance, since the dipolar interaction is inversely proportional to the cube of the distance, enabling measurement of larger distances [7]. Another advantage of the DQ coherence technique is that the measured signal has a preferential sensitivity to the dipolar interaction, since the DQ coherence is generated by it. As a consequence, the analysis of DQ coherence data to extract distances is cleaner that those from other techniques. For example, in the frequently used DEER (Double Electron Resonance) technique, one has to extract the weak dipolar echo modulation from the large echo decay background. As well, mono-radical impurities do not affect the DQ signal, unlike that with other techniques. The DQ method offers another advantage in that using it one can measure directly the double-quantum relaxation rate, T_2^D, the knowledge of which is very important to interpret motional dynamics.

Multi-pulse EPR has been frequently exploited for distance measurements in biological systems [8-19]. It is useful to have analytical expressions for the resulting pulsed EPR signals to keep track of the evolution of the various elements of the density matrix during the free evolution, as well as during the action of pulses, to follow how different coherence transfers are generated. On the other hand, it is easier to calculate pulsed EPR signals by numerical techniques, using the eigenvalues and eigenvectors of the pulse and static spin-Hamiltonian matrices, since the analytical expressions become lengthier and unwieldy to manipulate

numerically as the number of pulses increases. Besides, using them for calculation is susceptible to human error when transcribing the analytical expressions to numerical code.

This paper deals with a detailed study of coherence transfer for two-pulse DQ, as well as five-pulse DQM, which is an elaboration of the 2-pulse DQ sequence by introducing a refocusing π -pulse to enhance the signal, in samples containing nitroxide biradicals as spin probes, considering the dipolar interaction between the two nitroxide dipoles of the nitroxide biradical, as well as the fully asymmetric g and hyperfine matrices and the angular geometry of the biradical. Among others, it is focused on showing how to make the $p = 0$ to $p = 2$ DQ transition possible, which is forbidden for an infinite pulse, by using a finite pulse. In addition, we will discuss the important role the DQ transition plays in two-dimensional (2D) EPR, demonstrating the high sensitivity of the 2D-DQ EPR signals to the strength of the dipolar interaction and how to exploit it to measure orientational selectivity, as a result of constraints on the structural geometry, i.e., on the orientations of the dipolar axis of the two nitroxides of the biradicals. A full treatment of the problem will here be carried out, i.e., the calculation of Pake doublets in polycrystalline averages for the two-pulse DQ and five-pulse DQM signals, which are direct measures of the dipolar interaction, from which the distance between the two nitroxide dipoles in the nitroxide biradical used as spin probe, can be determined, being inversely proportional to the cube of the distance as $r = 10\big(51.9/d(MHz)\big)^{1/3}$, where d is the dipolar-coupling constant.

DQ transitions, which are forbidden for an infinite pulse and only possible by a finite pulse in conjunction with the dipolar interaction between the two nitroxides of a biradical, also provide orientational selectivity for smaller amplitudes of the irradiation field, B_1. This implies, as the analysis in this paper confirms, that the signal arises predominantly from those dipolar vectors, which are preferentially oriented symmetrically about the magic angle 54.74° at which $(3cos^2\theta - 1) = 0$.. Furthermore, the signal is also found to be sensitive to the orientations of the two nitroxide dipoles, useful for structural studies in biomolecules.

It is the purpose of this paper to carry out a thorough and complete treatment, performing all required numerical simulations, which can now be carried out on laptops equipped with very fast processors. Accordingly, we will derive (i) analytical expressions using Mathematica for two-pulse DQ and five-pulse DQM signals for an arbitrary orientation of the external magnetic field with respect to the dipolar axis required for studying orientational

selection, and (ii) to calculate, using Matlab, the polycrystalline (powder) signals using Monte-Carlo averaging over random orientations of the respective Euler angles of the two nitroxide dipoles with respect to the dipolar axis, needed to calculate the Pake doublets from their Fourier transforms. To this end, full numerical diagonalizations of the pulse- and spin-Hamiltonian matrices will be carried out, and the two-pulse DQ and five-pulse DQM signals will be calculated exploiting the algorithm of Misra et al. [8]. In addition, five-pulse DQM EPR signal will be simulated to fit the experimental data reported in [20]. The effect of relaxation on the powder averages will be considered by multiplying the final signal with a stretched exponential [21,22]. In addition, it will be shown here, from general considerations, that a finite, rather than infinite, pulse, in conjunction with the dipolar interaction, is needed to produce non-zero 0→2 and 2→-1 coherence transfers in the DQ experiment.

The organization of this paper is as follows. Section 2 deals with the required theoretical details, including the spin- and pulse-Hamiltonians for the nitroxide biradical and the solution of the Liouville von Neumann equation to calculate the signal, Derivation of full analytical expressions for two-pulse one-dimensional DQ and five-pulse DQM echo signals is given in detail in Sec. 3, including coherence transfer for the DQ and DQM signals. A discussion of the orientational selectivity and structural sensitivity of the coherence transfer, $T_{0\to2}$, is provided in Sec. 4. The numerical algorithm to simulate the two-pulse DQ and five-pulse DQM EPR signals for a polycrystalline sample, in the absence of relaxation, is provided in Sec 5. Calculation of the effect of relaxation on a polycrystalline sample, using a stretched exponential as described in [21,22], is discussed in Sec. 6. In Sec. 7 a discussion of the numerical results of the various simulations is presented. The conclusions are summarized in Sec. 8.

2. Theoretical Details

This section deals with the theory and the procedure to calculate the two-dimensional (2D) EPR signal for a coupled nitroxides biradical. One considers two dipolar-interaction coupled nitroxides, each characterized by an electron with spin $S = 1/2$ and a nucleus with spin $I = 1$. The dimension of the Hilbert space, in which the present calculations will be carried out, for such a system is 36x36, since $(2S_1 + 1)(2S_2 + 1)(2I_1 + 1)\ (2I_2 + 1)$=36, where the indices 1,2 refer to the two nitroxide. The effect of relaxation will be, for a polycrystalline

average, to multiply the calculated signal by a stretched exponential factor; more details are given in Sec. 4 below.

2.1 Spin Hamiltonian

For the coupled nitroxides the spin Hamiltonian is [7,8]

$$H_0 = H_{01} + H_{02} + H_{12} \tag{2.1}$$

where H_{0k}; *k=1,2,* denote the static Hamiltonians of the two nitroxide radicals, including the Zeeman and hyperfine interactions:

$$H_{0k} = C_k S_{z_k} + A_k S_{z_k} I_{z_k} + \frac{1}{2} B_k \, S_{z_k} I_{+_k} + \frac{1}{2} B_k{}^* S_{z_k} I_{-_k}; \quad k=1,2 \tag{2.2}$$

In Eq. (2.2), S_{z_k}, I_{z_k}, I_{+_k} and I_{-_k} are the spin operators for the two nitroxides, and the expressions for the coefficients C_k, A_k and B_k are given in Appendix A below. H_{12} in Eq. (2.1) includes the dipolar and exchange coupling between the two nitroxide radicals, expressed as

$$H_{12} = \frac{D}{2}(3cos^2\theta - 1)(S_z^2 - \boldsymbol{S}^2/3) + J\left(\frac{1}{2} - 2\,\boldsymbol{S_1}.\boldsymbol{S_2}\right) \tag{2.3}$$

where θ is the polar angle of the orientation of the static magnetic field with respect to the dipolar axis that connects the magnetic dipoles of the two nitroxides, J is the exchange-interaction constant between the two electrons, and D is the dipolar-interaction constant, expressed in terms of r, the distance between nitroxides, as [7,8].

$$D = \frac{3\gamma_e^2 \hbar}{2\mathrm{r}^3} \tag{2.4}$$

where γ_e is the gyromagnetic ration of the electron and $\hbar = h/2\,\pi$ is the reduced Planck's constant. The constant $d = 2/3\,D$ will be used hereafter, referred to as the "dipolar constant".

The Hamiltonian for the pulse of the radiation microwave magnetic field is expressed as [7,8]

$$H_p = \frac{\gamma_e B_1}{2}\left(e^{-I\phi} S_+ + e^{I\phi} S_-\right) \tag{2.5}$$

where B_1 is the amplitude of the pulse, $S_\pm$ are the raising/lowering operators of the total electronic spin of the coupled nitroxide system in the 36×36 direct product Hilbert space:

$$S_{\pm} = \sigma_{\pm_1} \otimes \mathbb{I}_{S_2} \otimes \mathbb{I}_{I_2} + \mathbb{I}_{S_1} \otimes \sigma_{\pm_2} \otimes \mathbb{I}_{I_1} \tag{2.6}$$

where $\otimes$ stands for the direct product, $\sigma_{\pm}$ are expressed in terms of the Pauli matrices σ_x and σ_y as $\sigma_{\pm} = \sigma_x \pm i\sigma_y$, $\mathbb{I}_{S_k}$, and $\mathbb{I}_{I_1}$; $k = 1,2$ are identity matrices in the electronic 2×2 and nuclear 9×9 spaces, respectively, of the two nitroxides. The magnetic basis described by the basis-vectors $|M_{S_1}, M_{S_2}, m_{I_1}, m_{I_2}\rangle$ is used hereafter, where $M_{S_1}, M_{S_2}, m_{I_1}, m_{I_2}$ denote the two electronic and the two nuclear magnetic quantum numbers, respectively, for the two nitroxides.

2.2 Initial density matrix. To calculate the signal for a multi-pulse sequence, one starts with the initial density matrix, ρ_0, governed by the Boltzmann distribution for two electrons each with spin ½ in thermal equilibrium. Using the high-temperature approximation and neglecting the energy-level modification by the hyperfine interaction, which is much less than the electronic Zeeman interaction, one can write:

$$\rho_0 = \frac{\left[\exp\left(-\widehat{H}_0/kT\right)\right]}{Tr\left[\exp\left(-\widehat{H}_0/kT\right)\right]} \propto \left(\mathbb{I} - \frac{\hbar\,\omega_0}{k_B T}\, S_Z + \cdots\right)$$

Since the final signal is obtained by taking the trace: $Tr(S_+\,\rho_f)$ and during the evolution of ρ_0 to ρ_f the term $\mathbb{I}$ remains invariant, it does not contribute to the signal as $Tr(S_+\,\mathbb{I}) = 0$. One can then replace ρ_0 , as follows:

$$\rho_0 \;\rightarrow S_Z \;= S_{z_1} + S_{z_2}$$

2.3 Calculation of pulsed EPR signal

The pulsed EPR signal for the system of coupled nitroxides, undergoing spin relaxation, is calculated by solving Liouville von-Neumann (LVN) equation that governs the time evolution of the density matrix during free evolution, i.e., in the absence of a pulse. It is expressed as [7-19]

$$\frac{d}{dt}\chi(t) = -i[H_0, \chi(t)] + \hat{\hat{\Gamma}}\,\chi(t) \tag{2.7}$$

where $\chi = \rho - \rho_0$ is the reduced density matrix, with $\rho_0 \propto S_{z_1} + S_{z_2}$, being the initial density matrix, as discussed in Sec. 2.2, and H_0 is given by Eq. (2.1). In Eq. (2.7), $\hat{\hat{\Gamma}}$ is the relaxation superoperator in Liouville space, whose matrix elements are:

$$\hat{\hat{\Gamma}}_{ij,kl} = -\delta_{ij}\delta_{kl}\frac{1}{(T_1)_{ik}} - \delta_{ik}\delta_{jl}\left(1-\delta_{ij}\right)\frac{1}{T_2^{S,D}}, \tag{2.8}$$

where $(T_1)_{ik}$ are the spin-lattice relaxation times between the populations *ii* to *kk*, which are operative on the coherent pathway $p = 0$, and $T_2^{S,D}$ are the spin-spin relaxation times operative along the $p = \pm 1$(index S), and $p = \pm 2$ (indexD) pathways, respectively, as shown in Fig. 1. It is noted that, in general, the spin-spin relaxation times, $\left(T_2^{S,D}\right)_{ij}$. are different for different transitions *ij*, but these relaxation times are only slightly different from each other as shown in [23]. As a consequence, they are all approximated here in Eq. (2.8) to have the same average spin-spin relaxation time $T_2^{S,D}$.

In the two-pulse DQ sequence, shown in Fig. 1, the pathway $p = 0$ is excluded, so that the relaxation times $(T_1)_{ik}$, with *i* = *k*, affecting the populations, that appear in Eq. (2.8) for the $p = 0$ pathway, have no effect on the signals. In the two-pulse sequence considered here, only the coherent pathways $p = \pm 1$ and $p = \pm 2$ participate, so that in the relaxation only the second term on the right-hand side of Eq. (2.8) which corresponds to $i \neq j$ elements of the reduced density matrix, affect the two-pulse DQ signal. Then, the solution of Eq. (2.7) after time t, expressing the evolution of χ_{ij} due to the relaxation along the $p = \pm 1, \pm 2$ pathways, is obtained as

$$\chi(t_0 + t) = e^{-t/T_2^{S(D)}} e^{-iH_0 t}\chi(t_0)\, e^{iH_0 t} \tag{2.9}$$

Appendix B below lists the elements of the matrix for $e^{-iH_0 t}$ used in Eq. (2.9) for the coupled nitroxides system.

As for the five-pulse DQM signal, which includes the coherence pathway $p = 0$ (Fig. 1), one also needs to consider the relaxation between the populations. To do that rigorously, one first needs to diagonalize the non-diagonal part of the relaxation matrix in Liouville space, as given by Eq. (2.8), which is a 36×36 matrix. At lower temperatures, used in the five-pulse experiment, the values of the off-diagonal elements of the relaxation matrix $(T_1)_{ik}$ in Eq. (2.8) for $i \neq k$, are larger than both the spin-spin relaxation times and the duration of the experiment by two order of magnitudes [24]; hence, they do not have any significant effect on the final signal and can thus be neglected. Keeping now only the diagonal elements of the relaxation matrix and assuming that

they are all equal to each other [23,24], the time evolution of the reduced density matrix on the coherence pathway $p = 0$ is

$$\chi(t_0 + t) = e^{-t/T_1} e^{-iH_0 t} \chi(t_0)\, e^{iH_0 t} \tag{2.10}$$

During the application of a pulse, the spin relaxation is here neglected, since the duration of the pulses are much smaller than the relaxation time. In that case, the evolution of the density matrix is described in Hilbert space, as follows:

$$\frac{d}{dt}\rho(t) = -i\big[(H_0 + H_p), \rho(t)\big] \tag{2.11}$$

with H_p being expressed by Eq. (2.5).

. The solution of Eq. (2.11), after the application of a pulse of duration t_p, neglecting relaxation during the pulse, is given as [7]:

$$\rho\big(t_0 + t_p\big) = e^{-i(H_0+H_p)t_p} \rho(t_0)\, e^{i(H_0+H_p)t_p} = P\, \rho(t_0)\, P^{\dagger} \tag{2.12}$$

In Eq. (2.12), † denotes the Hermitian adjoint of a matrix. The 36x36 matrix, P, for the propagator $P = e^{-i(H_0+H_p)t_p}$ in Eq. (2.12), has the general form in the electronic magnetic basis [7]:

$$\{\{P\}\} = \begin{pmatrix} [[P_{11}]] & [[P_{12}]]\, e^{-i\phi} & [[P_{13}]] e^{-i\phi} & [[P_{14}]] e^{-2i\phi} \\ [[P_{21}]] e^{i\phi} & [[P_{22}]] & [[P_{23}]] & [[P_{24}]] e^{-i\phi} \\ [[P_{31}]] e^{i\phi} & [[P_{32}]] & [[P_{33}]] & [[P_{34}]] e^{-i\phi} \\ [[P_{41}]] e^{2i\phi} & [[P_{42}]] e^{i\phi} & [[P_{43}]] e^{i\phi} & [[P_{44}]] \end{pmatrix} \tag{2.13}$$

where $[[P_{ij}]]$ are 9×9 matrices in the hyperfine space, with ϕ being the phase of the pulse as defined in Eq. (2.5). It is noted that for the coupled nitroxides system, considering the hyperfine interaction of the two nitroxides, each with nuclear spin $I = 1$, the 9×9 matrix elements of $[[P_{ij}]]$ in the hyperfine space of the propagator operator in Eq. (2.13) are rather long expressions, which can be calculated using Mathematica. They are not included here since all significant interpretations of relevance here can be made without fully listing them. *Hereafter, the double square brackets around* $[[P_{ij}]]$ *will be dropped, with the understanding that they are 9x9 matrices in the hyperfine space.*

After the application of a pulse, the density matrix is projected onto the coherence pathway of interest, which are: $p = 2, -1$ for DQ and 0, $\pm 1, 0, \pm 2, -1$ for DQM experiments, respectively, as given in Fig. 1. This is achieved by applying a projection operator that retains only the relevant elements of the density matrix which correspond to a particular pathway, p , putting all the other elements equal to zero. The projection operators for the various coherence pathways are given in Appendix C.

For the calculation of two-pulse DQ signals, the final density matrix $\rho_f(t_1, t_2)$, where t_1 is the time between the two pulses and t_2 is the time after the second pulse, at which the signal is recorded, as shown in Fig. 1, is obtained as follows. (i) Transform the initial density matrix by the first pulse using Eq. (2.12); (ii) Apply the relevant coherence pathway projection operator to the density matrix transformed in step (i); (iii) Calculate the density matrix after free evolution with relaxation of the density matrix obtained in step (ii) over the duration t_1 between the first and the second pulses using Eq. (2.9); (iv) Transform the density matrix obtained in step (iii) by the second pulse using Eq. (2.12); (v) Apply the coherence pathway projection operator for the coherence pathway $p = -1$ to the density matrix obtained in step (iv); (v) the final density matrix $\rho_f(\boldsymbol{t_1}, \boldsymbol{t_2})$ is obtained after free evolution with relaxation of the density matrix obtained in step (iv) over the time t_2.

For the five-pulse DQM, signals, the final density matrix $\rho_f(t_1, \ldots, t_5)$ with $t_k;\ k = 1, \ldots, 5$ being the time between the kth and $(k+1)$th pulse is obtained by successive applications of the 5 pulses to the initial density matrix, using Eq. (2.12), followed by the application of the relevant coherence pathway projection operator and then free evolutions over the coherence pathways as shown in Fig. 1, using Eqs. (2.9) and (2.10) for the coherence pathways $p = \pm 1, \pm 2$ and $p = 0$, respectively.

The complex signal, for the orientation, (θ, ϕ), of the static magnetic field relative to the dipolar axis that connects the magnetic dipoles of the two nitroxides for the orientation of the two nitroxide radicals, characterized by five independent Euler angles, $(\alpha_1 = 0, \beta_1, \gamma_1, \alpha_2, \beta_2, \gamma_2)$ (α_1 is chosen to be 0 since it is arbitrary), is then,

$$S^{(k)}(\{\boldsymbol{t_k}\}, \theta,\ \phi, \beta_1, \gamma_1, \alpha_2, \beta_2, \gamma_2) = Tr\big(S_+ \rho_f\{\boldsymbol{t_k}\}\big), \tag{2.14}$$

where $\{\boldsymbol{t_k}\}$, $k = 2$, 5 stand for t_1, t_2 and t_1, t_2, t_3, t_4, t_5 for the calculation of two-pulse and five-pulse signals, respectively.

Polycrystalline average. The EPR signal for a polycrystalline sample is calculated by integrating Eq. (2.13) over (θ, ϕ) covering only one quarter of the unit sphere (due to the symmetry) , as follows'

$$S^{(k)}(\{\boldsymbol{t_k}\}, \lambda_1, \lambda_2) = 4 \int_0^{\pi} d\phi \int_0^{\pi/2} S^{(k)}(\{\boldsymbol{t_k}\}, \eta, \lambda_1, \lambda_2)\, d(cos\ \theta) \tag{2.15}$$

In Eq. (2.14) the set of Euler angles, $(\alpha_1 = 0, \beta_1, \gamma_1); (\alpha_2, \beta_2, \gamma_2)$, and the orientation of the external magnetic field with respect to the dipolar axis (θ, ϕ) are denoted, respectively, as $\lambda_j; (j = 1,2)$ and η.

Calculation of Pake doublets. For this, one needs to average over the Euler angles λ_1, λ_2, the orientations of the dipoles of the two nitroxides. This is an enormous task as there are infinite many such possibilities. However, one can, instead, use Monte-Carlo averaging, wherein one varies λ_1, λ_2 randomly as follows:

$$S_{avg}^{(k)}(\boldsymbol{t_k}) = \sum_{\lambda_1, \lambda_2} S^{(k)}(\boldsymbol{t_k}, \lambda_1, \lambda_2) \tag{2.16}$$

Twenty such averaging were found to be sufficient, because another set of twenty Monte-Carlo averaging gave almost identical results.

Inhomogeneous Gaussian broadening due to precession of spins during the free evolution. In order to take into account the Gaussian inhomogeneous broadening effect, the final signals $S(\boldsymbol{t_k})$ in Eq. (2.13) for each orientation (θ, ϕ) are multiplied by the by the factors $e^{-2\pi^2 \Delta_G^2 (t_2 - 2t_1)^2}$ for two-pulse DQ [7] and $e^{-2\pi^2 \Delta_G^2 (t_5 - t_1)^2}$ for five-pulse DQM, where Δ_G is the Gaussian inhomogeneous broadening parameter.

Number of simulations. Thus, a total of 90 θ-values and 90 ϕ-values were used over a unit sphere, along with 20 sets of five Euler angles (λ_1, λ_2). This amounts to an average over $90 \times 90 \times 20 = 1.62 \times 10^5$ simulations. The procedure to calculate the two-pulse DQ or five-pulse DQM signal is described in the flowchart in Appendix D.

3. General procedure to derive analytical expressions for multi-pulse-EPR Signals.

In this section, a general algorithm to calculate the analytical expression for any pulse sequence is described. The calculation of the analytical expressions here is presented in the 4×4 electronic subspace, of which each element is a 9×9 matrix in the hyperfine subspace. To calculate the signal for an n-pulse sequence, one starts with the initial density matrix, ρ_0, which can be effectively reduced, for calculating the signal to as discussed in Sec. 2.2, as follows:

$$\rho_0 \rightarrow S_Z = S_{z_1} + S_{z_2} = diag\{1,0,0,-1\} \tag{3.1}$$

The density matrix, ρ, after the application of the first pulse, is obtained by using Eq. (2.12). After the application of a pulse, the density matrix on the coherence pathway of interest is obtained by applying the projection operator, P_k, defined in Appendix C, to the resulting density matrix, ρ. This is done by the Hadamard product, i.e. $\rho^{(k)} = P_k \circ \rho$, where P_k ; $k = 0, \pm 1, \pm 2$ is the projection operator for the coherence pathway $p = k$ and $\circ$ denotes the Hadamard product of two matrices, where each element i, *j* of the resulting density matrix is the product of the *i*, *j* of the projection operator matrix, P_k, and the element *i*, *j* of the 1 density matrix, ρ. In the absence of relaxation, the density matrix, after free evolution over time t on a coherence pathway, p, is found, by using Eqs. (2.9), (2.10) and (B.11), to be as follows:

For $p = 0$

$$e^{-IH_0 t}\rho^{(0)}e^{IH_0 t} = \begin{pmatrix} \rho_{11} & 0 & 0 & 0 \\ 0 & A & B & 0 \\ 0 & C & D & 0 \\ 0 & 0 & 0 & \rho_{44} \end{pmatrix} \tag{3.2}$$

where,

$$A \equiv S_1^{(0)}(t)\rho_{33} + S_2^{(0)}(t)\rho_{23} + S_2^{(0)}(t) * \rho_{32} + S_3^{(0)}(t)\rho_{22}$$
$$B \equiv S_1^{(0)}(t)\rho_{32} + S_2^{(0)}(t)(\rho_{22} - \rho_{33}) + S_4^{(0)}(t)\rho_{23}$$
$$C \equiv S_1^{(0)}(t)\rho_{23} - S_2^{(0)}(t) * \rho_{33} + S_2^{(0)}(t) * \rho_{22} + S_4^{(0)}(t) * \rho_{32}$$
$$D \equiv S_1^{(0)}(t)\rho_{22} + S_2^{(0)}(t)\rho_{23} - S_2^{(0)}(t) * \rho_{32} + S_3^{(0)}(t)\rho_{33}$$

For $p = +1$

$$e^{-IH_0t}\rho^{(+1)}e^{IH_0t} =$$

$$\begin{pmatrix} 0 & S_1^{(+1)}(t)\rho_{12} + S_2^{(+1)}(t)\rho_{13} & S_2^{(+1)}(t)\rho_{12} + S_5^{(+1)}(t)\rho_{13} & 0 \\ 0 & 0 & 0 & S_3^{(+1)}(t)\rho_{24} + S_4^{(+1)}(t)\rho_{34} \\ 0 & 0 & 0 & S_4^{(+1)}(t)\rho_{24} + S_6^{(+1)}(t)\rho_{34} \\ 0 & 0 & 0 & 0 \end{pmatrix} \tag{3.3}$$

For $p = +2$

$$e^{-IH_0t}\rho^{(+2)}e^{IH_0t} = \begin{pmatrix} 0 & 0 & 0 & S_1^{(+2)}(t)\rho_{14} \\ 0 & 0 & 0 & 0 \\ 0 & 0 & 0 & 0 \\ 0 & 0 & 0 & 0 \end{pmatrix} \tag{3.4}$$

where $\rho^{(0)}$, $\rho^{(+1)}$ and $\rho^{(2)}$ are the density matrices before the free evolutions, just after the application of the respective pulses, on the pathways $p = 0, +1, +2$, respectively, achieved by the application of the relevant projection operator. (Experimentally, it is achieved by phase cycling.) The $S^{(k)}{}_i(t); k = 0,1,2$ terms for free evolution over the various coherence pathways, used in Eqs. (3.2)-(3.4), are listed in Table I. The evolutions of the density matrix over the coherence pathways $p = -1$ and $p = -2$ are Hermitian adjoints of those for $p = +1$ and $p = +2$, respectively, as given above. The resulting density matrix at the end of a coherence pathway will serve as the starting density matrix to which the next pulse is applied. The same procedure is repeated for all other pulses in turn to calculate the final density matrix. The signal for a chosen orientations of the two nitroxide dipoles with respect to the dipolar axis, oriented at an angle θ with respect to the lab axis, is obtained using Eq. (2.14).

3.1 Analytical Expression for Two-pulse DQ signal

In this section, the DQ signal will be calculated analytically using the procedure outlined in Sec. 2 above. The pulse sequence for a DQ experiment is shown in Fig. 1(a). It consists of two finite arbitrary pulses each with the duration t_p. The phase cycling required for the pathways $p = 2$ and $p = -1$ in the two-pulse DQ sequence is given in Table II of [7]. Finite pulses, as opposed to infinite pulses, are needed to produce non-zero coherence transfers $T_{0\to 2}$ and $T_{2\to -1}$ as shown below, in general, in Sec. 3.3.2. For theoretical calculation, after the application of the first pulse, only the matrix elements corresponding to the double quantum coherence pathway $p = +2$ are retained in the density matrix, removing all the other matrix elements in it, using the appropriate projection operator. The system is then allowed to evolve freely with relaxation over time t_1

before the application of the second finite pulse, after which the coherence pathway $p = -1$ is chosen. wherein only the elements of the density matrix corresponding to the pathway $p = -1$ are retained, by using the appropriate projection operator. The signal is measured after time t_2 after the second pulse as shown in Fig. 1. It is noted that the tip angle $\beta = \gamma_e B_1 t_p$ for the pulses is a function of both the amplitude of the microwave field B_1 and the duration of the pulse. t_p, which determine the intensity of coherence transfer as shown in Sec. 3.3.2. Furthermore, it is the presence of the dipolar interaction only during a pulse that makes the non-zero coherence transfers possible.

Following the procedure described in Sec. 2, the DQ signal is calculated for a chosen orientation of the two nitroxide dipoles with respect to the dipolar axis, oriented at an angle θ with respect to the lab axis, to be as follows:

$$\begin{aligned}\text{Signal}^{\text{DQ}}(t_1, t_2) &= e^{i(3\phi_2 - 2\phi_1)}\text{Tr}\Big[NP_{14}^{(2)\dagger}S^*{}_1(t_2)P_{21}^{(2)} - P_{14}^{2\ \dagger}S^*{}_2(t_2)\Big(P_{21}^{(2)} + P_{31}^{(2)}\Big) \\ &+ P_{24}^{(2)\dagger}S^*{}_3(t_2)P_{41}^{(2)} - \Big(P_{24}^{(2)\dagger} + P_{34}^{(2)\dagger}\Big)S^*{}_4(t_2)P_{41}^{(2)} + P_{14}^{(2)\dagger}S^*{}_5(t_2)P_{31}^{(2)} \\ &+ P_{34}^{(2)\dagger}S^*{}_6(t_2)P_{41}^{(2)}\Big]e^{-t_1/T_2^D}e^{-t_2/T_2^S}e^{-2\pi^2\Delta_G^2(t_2-2t_1)^2}\end{aligned} \tag{3.5}$$

where the superscript (2) on the P_{ij} terms refer to the second pulse and the superscript $*$ denotes the complex conjugate of the S terms, given in Table I. In Eq. (3.5),

$$N = e^{-i\omega_{14}t_1}\Big(P_{11}^{(1)}P_{41}^{(1)\dagger} - P_{14}^{(1)}P_{44}^{(1)\dagger}\Big), \tag{3.6}$$

and the trace is taken over the 9×9 hyperfine space. In Eq. (3.6), $\omega_{14} = E_1 - E_4$ with $E_i; i = 1,2,3,4$, being the eigenvalues of the spin Hamiltonian, given in Appendix B. The superscripts $(1), (2)$ on the P_{ij} terms in Eqs. (3.5) and (3.6), refer to the first and second pulse, respectively. The 9×9 $S_i(t)$ and P_{ij}^k terms in Eq. (3.5) are given by Eq. (2.13) above.

3.2 Coherence transfer

It is important to have an estimate of the coherence transfer, since the intensity of the signal increases with increasing coherence transfer. The efficiency of the coherence transfer, $T_{m\to n}$, from the coherence pathway m to the coherence pathway n, is calculated as follows. The resulting density matrix for the pathway n by the application of a pulse to the density matrix is proportional to the spin operator corresponding to the coherence pathway n, which is S_z for the coherence pathway $p = 0$ for the initial density matrix, $S_{\pm}$ for the coherence pathways $p = \pm 1$ and $S_{\pm}.S_{\pm}$ for the coherence pathways $p = \pm 2$. The density matrix for the pathway n is then obtained by taking the trace of the density matrix resulting by the action of the pulse with the projection operator for the coherence pathway n, listed in Appendix C.

3.2.1 Coherence transfer efficiencies for 2-pulse DQ sequence for a finite pulse

The coherence transfer efficiency for the transitions 0→2 and 2→-1 in a DQ experiment is zero for an infinite pulse [7]. With the application of a finite pulse, however, one can obtain a non-zero $T_{0\to 2}$ and $T_{2\to -1}$.Using a rigorous analytical treatment, it is shown here that, indeed, $T_{0\to 2}$ and $T_{2\to -1}$are non-zero for the system of coupled nitroxides as effected by a pulse of finite duration, when there is present a non-zero dipolar interaction, seen as follows.

In the static Hamiltonian given by Eq. (2.1), H_{01} and H_{02} terms do not contribute to coherence transfer, because they contain the spin operator S_z, so only the dipolar-interaction term H_{12} need to be taken into consideration for the calculation of coherence transfer. In the magnetic basis of the two electrons, the matrix for H_0 in the direct-product space (see Appendix B), is then given as

$$H_0 \approx H_{12} = a\left(2S_z^2 - S_x^2 - S_y^2\right) = \begin{pmatrix} a & 0 & 0 & 0 \\ 0 & -a & -a & 0 \\ 0 & -a & -a & 0 \\ 0 & 0 & 0 & a \end{pmatrix} \tag{3.7}$$

where $a = \frac{3d}{4}(3cos^2\theta - 1)$. In the magnetic basis, the matrix of the pulse Hamiltonian together with the static Hamiltonian in the direct-product space is:

$$H_0 + H_p = \begin{pmatrix} a & \frac{1}{2}\omega e^{-i\phi} & \frac{1}{2}\omega e^{-i\phi} & 0 \\ \frac{1}{2}\omega e^{i\phi} & -a & -a & \frac{1}{2}\omega e^{-i\phi} \\ \frac{1}{2}\omega e^{i\phi} & a & -a & \frac{1}{2}\omega e^{-i\phi} \\ 0 & \frac{1}{2}\omega e^{i\phi} & \frac{1}{2}\omega e^{i\phi} & a \end{pmatrix} \tag{3.8}$$

whose eigenvalues, E_p and the eigenvectors, U, are given as

$$E_p = U^{\dagger}.\left(H_0 + H_p\right).U = \begin{pmatrix} 0 & 0 & 0 & 0 \\ 0 & \frac{1}{2}(\Omega - a) & 0 & 0 \\ 0 & 0 & \frac{-1}{2}(a + \Omega) & 0 \\ 0 & 0 & 0 & a \end{pmatrix} \tag{3.9}$$

where

$$U = \begin{pmatrix} 0 & -\frac{\omega}{\sqrt{9a^2 + 3\omega^2}} & \frac{\omega}{\sqrt{9a^2 + 3\omega^2}} & 0 \\ -\frac{1}{\sqrt{3}} & 0 & 0 & \frac{1}{\sqrt{3}} \\ \frac{1}{\sqrt{3}} & \frac{-a - \Omega}{2\sqrt{9a^2 + 3\omega^2}} & \frac{-a - \Omega}{2\sqrt{9a^2 + 3\omega^2}} & \frac{1}{\sqrt{3}} \\ \frac{1}{\sqrt{3}} & \frac{\Omega - a}{2\sqrt{9a^2 + 3\omega^2}} & \frac{\Omega - a}{2\sqrt{9a^2 + 3\omega^2}} & \frac{1}{\sqrt{3}} \end{pmatrix} \tag{3.10}$$

$$\Omega = \sqrt{9a^2 + 4\omega^2}$$

Then the pulse propagator, including the static Hamiltonian, is expressed as

$$e^{-I(H_0 + H_p)t_p} = U.e^{-IE_p t_p}.U^{\dagger} \tag{3.11}$$

Following the procedure to calculate the coherence transfer as given in Sec. 3.2 below and using the pulse propagator, given by Eq. (3.11), the coherence transfer for the transition 0 → 2, $T_{0\to 2}$ is found to be:

$$T_{0\to 2} = Tr\left[S_+ . S_+ . e^{-I(H_0+H_p)t_p} . S_z . e^{I(H_0+H_p)t_p}\right]$$
$$= \frac{i}{2}\left(\sin\left(\frac{at_p}{2}\right)\cos\left(\frac{1}{2}\Omega t_p\right) - \frac{a\cos\left(\frac{at_p}{2}\right)\sin\left(\frac{1}{2}\Omega t_p\right)}{\Omega}\right) \quad (3.12)$$

and for the transition $2 \to -1$, the coherence transfer is:

$$T_{2\to -1} = Tr\left[S_+ . e^{-I(H_0+H_p)t_p} . (S_+ . S_+) . e^{I(H_0+H_p)t_p}\right]$$
$$= \frac{\omega \sin\left(\frac{1}{2}\Omega t_p\right)\left(a\sin\left(\frac{1}{2}\Omega t_p\right) - \Omega\sin\left(\frac{a\, t_p}{2}\right)\right)}{\Omega^2} \quad (3.13)$$

It is noted from Eqs. (3.12) and (3.13) that when either the dipolar coupling, or the pulse, is zero both the coherence transition $T_{0\to 2}$ and $T_{2\to -1}$ vanish, since a is proportional to the dipolar constant d and ω is proportional to B_1.

3.3 One-dimensional Signals for DQ and DQM sequences

It is shown in Secs. 3.3.1 and 3.3.2 below, that the signal is maximum for $t_2 = 2t_1$ for two-pulse DQ sequence, whereas it is maximum for $t_5 = t_1$ for five-pulse DQM sequence, respectively. Thus, one can use one-dimensional (1D) measurements along these equal times, instead of varying them independently, to measure Pake doublets to obtain the value of the dipolar interaction constant, which is inversely proportional to the cube of the distance between the two nitroxides of the biradical.

3.3.1 One-dimensional-two-pulse DQ signal

It is seen from the analytical expressions in Eq. (3.5) that the time-dependent parts of the DQ signals at times t_1 and t_2, specified by $S_m(t_1), S_m(t_2)^*, m = 1, \ldots, 6$, given in Table I, contain the terms $e^{-i\omega_{ij}t_1}$ and $e^{i\omega_{ij}t_2}$, respectively, where $\omega_{ij} = (E_i - E_j)/\hbar$; where the E_i, and E_j are defined by Eq. (B.10) in Appendix B below. In the rotating frame, the value of $|C_1 - C_2|^2$ and $|(A_1^2 + 4|B_1|^2)^{1/2} - (A_2^2 + 4|B_2|^2)^{1/2}|^2$ terms appearing in the E_i and E_j, become negligible compared to $\left(d(3cos^2\theta - 1)\right)^2$ for large dipolar interaction i.e. $d \geq 10$ MHz. The explicit expressions for ω_{ij} are then:

$$\hbar\omega_{12} = \frac{1}{2}\left(j\sqrt{A_1^2 + 4B_1^2 j} + k\sqrt{A_2^2 + 4B_2^2 k} + C_1 + C_2 + \frac{3}{2}d(3\cos^2\theta - 1)\right)$$
$$\hbar\omega_{13} = \frac{1}{2}\left(j\sqrt{A_1^2 + 4B_1^2 j} + k\sqrt{A_2^2 + 4B_2^2 k} + C_1 + C_2 + \frac{1}{2}d(3\cos^2\theta - 1)\right)$$
$$\hbar\omega_{24} = \frac{1}{2}\left(j\sqrt{A_1^2 + 4B_1^2 j} + k\sqrt{A_2^2 + 4B_2^2 k} + C_1 + C_2 - \frac{3}{2}d(3\cos^2\theta - 1)\right)$$
$$\hbar\omega_{34} = \frac{1}{2}\left(j\sqrt{A_1^2 + 4B_1^2 j} + k\sqrt{A_2^2 + 4B_2^2 k} + C_1 + C_2 - \frac{1}{2}d(3\cos^2\theta - 1)\right)$$
$$\hbar\omega_{14} = j\sqrt{A_1^2 + 4B_1^2 j} + k\sqrt{A_2^2 + 4B_2^2 k} + C_1 + C_2 \qquad (3.15)$$

After substituting the various ω_{ij} terms given by Eq. (3.15) and $S_i(t_k);\ i = 1, \ldots, 6;\ k = 1,2$, given in Table I, the expressions for the DQ signal, as given by Eq. (3.5), can be written as

$$\begin{aligned}
&\mathrm{DQ}^{\mathrm{Signal}}(t_1, t_2) = e^{i(3\phi_2 - 2\phi_1)} e^{-t_1/T_2^D} e^{-t_2/T_2^S} e^{-2\pi^2\Delta_G^2(t_2 - 2t_1)^2} \\
&\times \mathrm{Tr}[N\{F_-\, {P_{14}^2}^{\dagger}(P_{31}^2 cos\,\Xi - P_{21}^2 sin\,\Xi)\, e^{i\left(\frac{1}{4}d.(3\cos^2\theta - 1)t_2 + \frac{1}{2}(2t_1 - t_2)\mathrm{ZHF}\right)} \\
&+F_+ {P_{14}^2}^{\dagger}(P_{21}^2 cos\Xi + P_{31}^2 sin\Xi) e^{i\left(\frac{3}{4}d.(3\cos^2\theta - 1)t_2 + \frac{1}{2}(2t_1 - t_2)\mathrm{ZHF}\right)} \\
&+F_- P_{41}^2 \left(cos\Xi {P_{34}^2}^{\dagger} - sin\Xi {P_{24}^2}^{\dagger}\right) e^{i\left(-\frac{1}{4}d.(3\cos^2\theta - 1)t_2 + \frac{1}{2}(2t_1 - t_2)\mathrm{ZHF}\right)} \\
&+F_+ P_{41}^2 \left(cos\Xi\, {P_{24}^2}^{\dagger} + sin\Xi\, {P_{34}^2}^{\dagger}\right) e^{i\left(-\frac{3}{4}d.(3\cos^2\theta - 1)t_2 + \frac{1}{2}(2t_1 - t_2)\mathrm{ZHF}\right)}\}]
\end{aligned} \qquad (3.16)$$

where

$$\begin{aligned}
\mathrm{ZHF} &= j\sqrt{A_1^2 + 4B_1^2 j} + k\sqrt{A_2^2 + 4B_2^2 k} + (C_1 + C_2) \\
F_- &= \cos\Xi - \sin\Xi, \\
F_+ &= \cos\Xi + \sin\Xi.
\end{aligned} \qquad (3.17)$$

It is seen from Eq. (3.16) that, for $t_2 = 2t_1$, the effect of Zeeman and hyperfine interactions, as well as the Gaussian inhomogeneous broadening, in the time-dependent part of the signal, will become zero. leaving the time-dependent part of the DQ signal with the terms $e^{\pm\frac{id(3cos^2\theta - 1)}{4}2t_1}$ and

$e^{\pm\frac{3id(3cos^2\theta-1)}{4}2t_1}$ along with the exponential factor due to the relaxation. By choosing $t_2 = 2t_1$, only one variable time is needed, and the 2D DQ signal reduces to 1D signal.

It is seen from Eqs. B.6 and B.8 in Appendix B that, when the dipolar interaction is large, i.e., $\frac{d}{4}(3cos^2\theta - 1) \gg |C_1 - C_2|$, $d(3cos^2\theta - 1) \gg \left|(A_1^2 + 4|B_1|^2)^{1/2} - (A_2^2 + 4|B_2|^2)^{1/2}\right|$, one can then make the approximation $H_{22} \approx H_{33}$ for which yields $\Xi \approx \pi/4$. The F_- factor in Eq. (3.17) then becomes zero, and the reduced 1D DQ signal$(t_2 = 2t_1)$ can now be expressed as

$$\mathrm{DQ}^{\mathrm{Signal}}(t_1, t_2) = e^{i(3\phi_2 - 2\phi_1)} e^{-t_1/T_2^D} e^{-2t_1/T_2^S}$$
$$\times \mathrm{Tr}\left[N\left\{\left(P_{24}^{2\,\dagger} + P_{34}^{2\,\dagger}\right)P_{41}^2\, e^{-i\frac{3}{2}d\times(3\cos^2\theta-1)t_1} + P_{14}^{2\,\dagger}(P_{21}^2 + P_{31}^2)e^{+i\frac{3}{2}d\times(3\cos^2\theta-1)t_1}\right\}\right] \quad (3.18)$$

An examination of Eq. (3.18) reveals that the signal depends on $\pm\frac{3d}{2}\times(3cos^2\theta - 1)t_1$, whose Fourier transform as a function of t_1 would yield a peak at the frequencies $\pm\frac{3d}{2}\times(3cos^2\theta - 1)$ for the orientation of the magnetic field at angle θ with the dipolar axis connecting the two nitroxide dipoles. When the average is calculated over θ, ϕ for any choice of the five independent Euler angles, the orientations with $\theta\sim\pi/2$ contribute predominantly to the polycrystalline averaging because of the weighting factor of $sin\,\theta$ in the powder average, which implies that the peak of the signal, i.e., the Pake doublet, will occur at $\pm\frac{3d}{2}$ when averaged over the five independent Euler angles defining the orientations of the two nitroxide dipoles.

3.3.2 One-dimensional Five-pulse DQM signal

The five-pulse DQM pulse sequence is shown in Fig 1(b). In this sequence, the first pulse $(\pi/2)_x$ moves the density matrix to the single-quantum coherence pathway ($p = +1$), over which it evolves for a period t_1. The second finite $(\pi)_x$ pulse transfers this magnetization to $p = 0$ coherence pathway and the density matrix evolves on it over the period t_2. Thereafter, the third pulse transfers the density matrix to the double quantum $(p = \pm 2)$ coherence pathways, over which the density matrix undergoes free evolution for the time interval t_3. It is then subjected to the fourth, refocussing pulse $(\pi)_x$. After the time interval t_4 on the coherence pathways $p = \pm 2$, the fifth $(\pi/2)_x$ pulse finally transfers the density matrix to the single quantum coherence pathway $p = -1$, on which the signal is detected after the time interval t_5. In the experiment, t_1=t_2 , which

are stepped. As well, $t_3 = t_4$ which will here be denoted for this pulse sequence as $t_{DQ}^{(DQM)}$; it is kept fixed. The echo in this five-pulse DQM sequence occurs at the time $t_5 = t_1$.

The five-pulse DQM sequence, shown in Fig. 1(b), is equivalent to two coherence pathways, both of which lead to the formation of an echo at $t_5 = t_1$. These are:

$$\text{(i)} \qquad p = 0 \to +1 \to 0 \to +2 \to -2 \to -1 \tag{3.19}$$
$$\text{(ii)} \qquad p = 0 \to +1 \to 0 \to -2 \to +2 \to -1$$

In the above, for the partial pathways $0 \to +2$ and $0 \to -2$ in (i) and (ii), respectively, finite pulses are used for the indicated coherence transfers, otherwise for the remaining pathways infinite pulses are used.

Following the procedure described in Secs. 2 and 3, the 1D five-pulse DQM signals for the two coherence pathways in Eq. (3.19) are calculated for $t_5 = t_1$, for chosen orientations of the two nitroxide dipoles with respect to the dipolar axis, oriented at an angle θ with respect to the lab axis, respectively, to be as follows:

$$\text{Signal}_{DQM}^{(i)}(t_1) = \frac{1}{4} e^{-i(\phi_1 - \phi_2 + 2\phi_3 - 4\phi_4 + \phi_5)} e^{-2t_{DQ}^{(DQM)}/T_2^D} e^{-2t_1/T_2^S} e^{-t_1/T_1} e^{-2\pi^2 \Delta_G^2 (t_5 - 2t_1)^2}$$
$$\times Tr\left[\left(P_{11}^3 M_1 P_{14}^{2\,\dagger} P_{41}^{3\,\dagger} + P_{14}^3 M_2 P_{44}^{2\,\dagger} P_{44}^{3\,\dagger} + (P_{12}^3 M_3 + P_{13}^3 M_4)\left(P_{24}^{2\,\dagger} P_{42}^{3\,\dagger} + P_{34}^{2\,\dagger} P_{43}^{3\,\dagger}\right)\right) e^{id(3\cos^2\theta - 1)t_1} - \left(P_{11}^3 P_{11}^2 M_1^{\dagger} P_{41}^{3\,\dagger} + P_{14}^3 P_{41}^2 M_2^{\dagger} P_{44}^{3\,\dagger} + (P_{12}^3 P_{21}^2 + P_{13}^3 P_{31}^2)\left(M_3^{\dagger} P_{42}^{3\,\dagger} + M_4^{\dagger} P_{43}^{3\,\dagger}\right)\right) e^{-id(3\cos^2\theta - 1)t_1}\right] \tag{3.20a}$$

$$\text{Signal}_{DQM}^{(ii)}(t_1) = -\frac{1}{4} e^{-i(\phi_1 - \phi_2 - 2\phi_3 + 4\phi_4 + 3\phi_5)} e^{-2t_{DQ}^{(DQM)}/T_2^D} e^{-2t_1/T_2^S} e^{-t_1/T_1}\, e^{-2\pi^2 \Delta_G^2 (t_5 - 2t_1)^2}$$
$$\times \text{Tr}\left[\left(P_{41}^3 M_1 P_{14}^{2\,\dagger} P_{11}^{3\,\dagger} + P_{44}^3 M_2 P_{44}^{2\,\dagger} P_{14}^{3\,\dagger} + (P_{42}^3 M_3 + P_{43}^3 M_4)\left(P_{34}^{2\,\dagger} P_{13}^{3\,\dagger} + P_{24}^{2\,\dagger} P_{12}^{3\,\dagger}\right)\right) e^{id(3\cos^2\theta - 1)t_1} - \left(P_{41}^3 P_{11}^2 M_1^{\dagger} P_{11}^{3\,\dagger} + P_{44}^3 P_{41}^2 M_2^{\dagger} P_{14}^{3\,\dagger} + (P_{42}^3 P_{21}^2 + P_{43}^3 P_{31}^2)\left(M_3^{\dagger} P_{12}^{3\,\dagger} + M_4^{\dagger} P_{13}^{3\,\dagger}\right)\right) e^{-id(3\cos^2\theta - 1)t_1}\right] \tag{3.20b}$$

The five-pulse DQM signal, combining the ones due to the two simultaneous coherence pathways (i) and (ii), is then:

$$\text{Signal}_{DQM}(t_1) = \text{Signal}^{(i)}_{DQM}(t_1) + \text{Signal}^{(ii)}_{DQM}(t_1) \tag{3.21}$$

It is seen from Eq. (3.20) that the main dipolar peaks for a chosen orientation of the two nitroxide dipoles with respect to the dipolar axis, oriented at an angle θ with respect to the lab axis, will occur in the Fourier transform at $\pm d \times (3\cos^2\theta - 1)$. This shows that similar to the 1D two-pulse DQ case in Sec. 3.3.1, the Pake doublet for the 1D five-pulse DQM signal, will occur at $\pm d$ when averaged over the five independent Euler angles defining the orientations of the two nitroxide dipoles.

4. Orientational selectivity and elucidation of structure of biomolecules in 2-pulse DQ and 5-pulse DQM signals

4.1 Orientational selectivity. It is first noted that the forbidden transition $p = 0 \rightarrow 2$ in the two-pulse DQ and five-pulse DQM sequences becomes possible only in the presence of the dipolar interaction and a for a finite pulse. When this condition is satisfied, then the coherence transfer $T_{0\rightarrow 2}$ is much larger in a very narrow range about four specific values of θ, the angle between the dipolar axis and the external magnetic field. Then, there occurs ***orientational selectivity***. These specific four angles depend on the amplitude of the irradiation field, B_1, and the dipolar interaction, d, as the simulations presented here show. It implies that the signal arises predominantly from those dipolar vectors which are oriented parallel, or nearly parallel, to about $\pm 10^\circ$ from the magic angle, 54.74° at which $(3cos^2\theta - 1) = 0$, and its supplementary angle 125.26°. This results in the signal being very sensitive to both the dipolar interaction, and therefore the inter-electron distance in the nitroxide biradicals, since the dipolar interaction is proportional to the inverse cube of the distance between the two magnetic dipoles, and the orientation, θ, of the dipolar axis with respect to the external magnetic field. To illustrate this, simulations are carried out here for $T_{0\rightarrow 2}$ for four values of d = 10, 20, 30, and 40 MHz as shown in Figs. 3(a), 3(b), 3(c), 3(d), respectively, for varying values of B_1. It is found from these figures that for smaller B_1 and larger d, i.e., d = 20, 30, 40 MHz there are, indeed, two such values in the range $0^\circ \leq \theta_0 \leq 90^\circ$, for which the $T_{0\rightarrow 2}$ value is much larger than those for other values of θ. These values are found to be situated symmetrically within 10° away from the magic angle 54.74° at which $(3cos^2\theta - 1) = 0$, becoming closer to the magic angle as d increases, as seen from Figs. 3(b),

3(c) and 3(d), giving rise to orientational selectivity. implying that these spins will be preferentially pumped from $p = 0$ to $p = 2$ coherence state. ***This is a first-ever novel result, as far as orientational sensitivity is concerned,*** found with the help of extensive quantitative simulations for the first time. This orientational selectivity of the forbidden DQ signal occurs for d > 10 MHz up to a maximum value of B_1 that depends on d.. As for $20\ MHz \leq d \leq 40\ MHz$, it occurs for $B_1 \leq 3.0$ G for both two-pulse DQ and five-pulse DQM sequences. It is noted that there is no orientational selectivity possible for $d \leq 10$ MHz.

4.2 Elucidation of structure of biomolecules. As seen from the simulations made here for different sets of Euler angles, defining the orientations of the two magnetic dipoles of the nitroxide bilabel, in Sec 7 below, the signals from two-pulse DQ and five-pulse DQM sequences are found to be sensitive to the orientations of the two nitroxide dipoles, as described by the Euler angles $(\alpha_1, \beta_1, \gamma_1)$; $(\alpha_2, \beta_2, \gamma_2)$. This provides structural sensitivity to the two-pulse DQ and five-pulse DQM signals, useful for understanding details of the configuration of biomolecules.

5. Numerical simulations in the absence of relaxation

Although analytical expressions are useful in deducing important features of the signal and its Fourier transform, they are susceptible to human error when transcribing them into a code for numerical calculation. Therefore, the best way to calculate pulsed EPR signals is by numerical techniques using the eigenvalues and eigenvectors of the Hamiltonian matrix. The details of the calculations presented in this section, based on the algorithm developed by Misra to calculate the six-pulse DQC signal [8], are quite general, applicable to both one- and two- dimensional two-pulse DQ and five-pulse DQM signals.

In the numerical calculations performed here, the magnetic basis with the basis vectors $\left|M_{s_1}, M_{s_2}, m_{I_1}, m_{I_2}\right\rangle$ is used to calculate the various matrix elements. Here $M_{s_1}, M_{s_2}, m_{I_1}, m_{I_2}$ are the two electronic and the two nuclear magnetic quantum numbers, respectively, for the two nitroxides. In this magnetic basis, the static Hamiltonian H_0 is not diagonal; the eigenvalues of H_0 are obtained by the diagonalization $U^{\dagger} H_0 U = E$, where E is the eigenvalue matrix, whose diagonal elements are the eigenvalues, whereas the columns of matrix U are the corresponding eigenvectors.

To calculate the k-pulse signal, one starts with the initial density matrix, which is S_Z as discussed in Sec. 3, in the direct-product space: $\rho_0 \rightarrow S_Z = \left(\frac{\sigma_{Z_1}}{2}\right) \otimes \mathbb{I}_{S_2} \otimes \mathbb{I}_{I_1} \otimes \mathbb{I}_{I_2} +$

$\mathbb{I}_{S_1} \otimes \left(\frac{\sigma_{z_2}}{2}\right) \otimes \mathbb{I}_{I_1} \otimes \mathbb{I}_{I_1}$, where σ_{z_i} ; $i = 1,2$ are the Pauli spin matrices for the electron spin. The final density matrix $\rho_f(\{\boldsymbol{t_k}\})$ with k=2,5 for two- and five-pulse signals, respectively, is obtained by successive applications of the k pulses to it using Eq. (2.12), followed by free evolutions over the coherence pathways as shown in Fig. 1 for each pulse sequence using Eqs. (2.9) and (2.10) without the exponential factor that considers the effect of relaxation. The complex signal is then obtained using Eq. (2.14). The polycrystalline average and Pake doublets are calculated using Eqs. (2.15) and (2.16), respectively. Thereafter, the relevant Gaussian inhomogeneous broadening factor is multiplied to Eq. (2.16) for Pake doublets, as discussed in Sec.2, The flow chart for simulations is given in Appendix D.

6. Relaxation in a polycrystalline sample

In Sec. 4. above, the signal for a polycrystalline sample is calculated in the absence of relaxation. To consider the effect of the relaxation for a powder average, the *stretched exponential* approach is used here, following the discussion in [21,22], which considers the average effect of different relaxation times for different orientations of the dipolar axis with respect to the magnetic field by a single exponential with the exponent β. For the present cases this is discussed as follows.

Averaging over relaxation times $\boldsymbol{T_1}$, $\boldsymbol{T_2^S}$ and $\boldsymbol{T_2^D}$. According to Eqs. (2.9) and (2.10), after time t, for a single-orientation of the dipolar axis with respect to the external magnetic field, the effect of relaxation on the signal is considered by multiplying the calculated signal by the exponential factors $exp(-t/T_2^S)$, $exp(-t/T_2^D)$ and $exp(-t/T_1)$ for the coherence pathways $p = \pm 1$, $p = \pm 2$ and $p = 0$, respectively, with the time constants T_2^S, T_2^D, T_1, appropriate for that orientation. Then the cumulative effect of the relaxation on the multi-pulse signals, considering all coherence pathways as shown in Fig. 1, is calculated by multiplying the signal with two and five decaying exponential functions for two-and five-pulse sequences, respectively. For a polycrystalline sample, the signal is averaged over different values of (θ, ϕ), each characterized by different relaxation times $T_1(\eta, \lambda_1, \lambda_2)$ $T_2^S(\eta, \lambda_1, \lambda_2)$, $T_2^D(\eta, \lambda_1, \lambda_2)$. The effect of relaxation at the top of the echo, i.e., at $t_2 = 2t_1$ for two-pulse DQ and at $t_5 = t_1$ for five-pulse DQM, is expressed as

$$S(\boldsymbol{t_k})_{Avg} = \sum_{\eta,\lambda_1,\lambda_2} S_0(\boldsymbol{t_k},\eta,\lambda_1,\lambda_2)\, exp\left(-t_1\left(1/T_2^D(\eta,\lambda_1,\lambda_2) + 2/T_2^S(\eta,\lambda_1,\lambda_2)\right)\right) for\ DQ$$

$$S(\boldsymbol{t_k})_{Avg} = \sum_{\eta,\lambda_1,\lambda_2} S_0(\boldsymbol{t_k},\eta,\lambda_1,\lambda_2)\, exp\left(-2t_{DQ}^{(DQM)}/T_2^D(\eta,\lambda_1,\lambda_2) - t_1(2/T_2^S(\eta,\lambda_1,\lambda_2) + 1/T_1(\eta,\lambda_1,\lambda_2)\right)\ for\ DQM \quad (6.1)$$

where $S_0(\boldsymbol{t_k},\eta,\lambda_1,\lambda_2)$ is the EPR signal calculated without relaxation as given by Es. (2.14). Assuming the same orientational distribution function for the three relaxation times $T_1(\eta,\lambda_1,\lambda_2), T_2^S(\eta,\lambda_1,\lambda_2)$ and $T_2^D(\eta,\lambda_1,\lambda_2)$ over $(\eta,\lambda_1,\lambda_2)$, Eq. (6.1), becomes modified, as follows [21,22]:

$$S^{DQ}{}_{0\,Avg}(\boldsymbol{t_k}) = S_{0\,Avg}(\boldsymbol{t_k})\, exp\left(-[t_1(1/T_{2str}^D + 2/T_{2str}^S)]^{\beta}\right) \quad (6.2a)$$

$$S^{DQM}{}_{0\,Avg}(\boldsymbol{t_k}) = S_{0\,Avg}(\boldsymbol{t_k})\, exp\left(-\left[2t_{DQ}^{(DQM)}/T_{2str}^D + t_1(2/T_{2str}^S + 1/T_{1str})\right]^{\beta}\right) \quad (6.2b)$$

where, $S_{0\,Avg}(\boldsymbol{t_k})$ is the average of $S_0(\boldsymbol{t_k},\eta,\lambda_1,\lambda_2)$ over all orientations $(\eta,\lambda_1,\lambda_2)$ as described by Eqs (2.15) and (2.16) and T_{1str}, $T_{2\,str}^S$ and $T_{2\,str}^D$ are the stretched relaxation times over zero ($p = 0$), single ($p = 1$ pathway) and double ($p = 2$ pathway) quantum states, respectively. The stretching parameter, β, which is related to the distribution function of the relaxation times in Eqs. (6.2a) and (6.2b) ranges between zero and one [21,22]. Equations (6.2a) and (6.2b) reduce to a system with orientation-independent relaxation times in the limit when $\beta \rightarrow 1$. It is noted that, in general, there are two different stretching parameters, $\beta^{(S)}$and $\beta^{(D)}$, characterizing the orientational distribution of the single and double quantum relaxation times which are to be found by fitting the simulation to the experimental data [21,22]. In this paper, since the experimental values for $\beta^{(S)}$and $\beta^{(D)}$ are not available, and $\beta^{(D)}$ affects only the intensity of the signal, the value $\beta^{(S)}=\beta^{(D)} = \beta = 0.8$ is used, being the average of the two values 0.78 and 0.85 used in [21,22].

7. Discussion of results of numerical simulations

For reference, the values and definitions of the constants used in the numerical simulations are listed in Table I below. The simulations for the polycrystalline sample were carried out over a 90×90 $\{\cos\theta, \phi\}$ grid on the unit sphere for 20 different sets of five Euler angles $\{(0, \beta_1, \gamma_1), (\alpha_2, \beta_2, \gamma_2)\}$ with Monte-Carlo averaging to calculate the Pake doublets. In the numerical

simulations for distance measurement carried out here, only one variable time is used to calculate 1D signals, specifically for $t_2 = 2t_1$ for two-pulse DQ and $t_5 = t_1$ for five-pulse DQM signals. This results in a considerable saving of time in experimental measurements. As well, the simulations for a polycrystalline sample can be carried out using a much larger grid over the unit sphere because only a single time variable is needed.

7.1 Two-pulse DQ signal.

The maint features of the simulation for the coherence transfer for the DQ signal are as follows.

(i) Figure 2 displays the dependence of the1D time-domain DQ signals on the dipolar constant for three different values of the dipolar-coupling constant $d = 10, 20. 30$ MHz, simulated for $t_1$with $t_2 = 2t_1$, along with their Fourier transforms as a function of t_1. The magnitude of the radiation microwave field $B_1 = 10G$ and the duration of the finite pulses $t_p = 80$ ns The Pake doublets in the Fourier transform of DQ signals, indeed, appear at $\pm 3d/2$ as deduced from Eq. (3.18).

(ii) Using the analytical expression given by Eq. (3.12), the coherence transfer $T_{0\to 2}$ is plotted in Fig. 3 as function of θ for different values of the amplitude of the irradiation field, B_1 , for (a) $d = 10$ MHz, (b) $d = 20$ MHz, (c) $d = 30$ MHz and (d) $d = 40$ MHz. The duration of the pulse t_p for each value of B_1 is chosen so that the pulse becomes a nominal $\pi/2$ pulse. It is seen that the coherence transfer is zero at $\theta_0 = 54.74^\circ$ i.e., the value which make $(3cos^2(\theta) - 1) = 0$, for any values of d and B_1. The maximum orientational selectivity are found to occur at lower values of B_1 and higher values of d which are situated symmetrically within 10° about θ_0. All the plots are symmetric with respect to $\theta = 90^\circ$.

(iii) The Fourier transform of the DQ time signal for two sets of the Euler angles:(a) $(\alpha_1, \beta_1, \gamma_1) = (0,2\pi/3,0), (\alpha_2, \beta_2, \gamma_2) = (0, \pi/6,0)$;(b) $(\alpha_1, \beta_1, \gamma_1) = (0, \pi/4,0), (\alpha_2, \beta_2, \gamma_2) = (0, \pi/6,0)$ are shown in Fig. 4, calculated for $d = 20$ MHz and $B_1 = 10.0\, G$. The Fourier transforms of the DQ signal, as compared to other two-pulse signal such as COSY/SECSY (not shown here), are more sensitive to the relative orientations of the nitroxide radicals, making the DQ experiment more suitable for structural studies of the coupled nitroxide biradical.

(iv) The effect of relaxation on DQ signal is shown in Fig. 5, displaying the Fourier transform of the DQ signal without and with relaxation, calculated with the relaxation times $T_2^S =$

500 ns (over the pathways $p = \pm 1$) and $T_2^D = 200$ ns (over the pathways $p = \pm 2$), $d = 40$ MHz and $B_1 = 10.0\ G$. As expected, the Pake doublets become broadened by relaxation. Furthermore, T_2^D has more dominant contribution as compared to that of T_2^S , as its value is almost half that of T_2^Sas determined experimentally in [20], since the relaxations factors are inversely proportional to the exponential of the relaxation time.

(v) The efficiencies of the coherence transfers for the transitions 0 → 2 and 2 → -1 in the DQ two-pulse experiment are plotted in Figs. 6 and 7 as functions of (B_1, t_p) for the values of the dipolar constant $d = 10$ and 30 MHz, respectively. They show that the value of the coherence transfer in the DQ experiment for the transition 0 → 2 is almost twice of that for the transition 2 → -1. Furthermore, coherence transfers are significantly affected by the dipolar interaction; specifically, the efficiency of the coherence transfer in the transition 0→2 increases from 0.06 for $d = 10$ MHz to 0.12 for $d = 30$ MHz. This is in accordance with the predictions of Eqs. (3.12) and (3.13), giving the theoretical expressions for these two coherence transfers, which imply that with larger *d* there is greater coherence transfer.

7.2 Five-pulse DQM signal

The relevant features of the simulations for the coherence transfer for the DQM signal are as follows.

(i) The Pake doublets in the Fourier transforms of the DQM signals, indeed, appear at $\pm d$ as deduced from Eq. (3.20), as seen from Fig 8, which displays the dependence of the time-domain DQM signals on the dipolar constant for *d = 10, 20, 30 MHz*, simulated for $t_5 = t_1$, along with their Fourier transforms as functions of t_1. The amplitude of the radiation microwave field is B_1=17.8 G, the same as that used in [20]. The durations of the pulses are $(t_p)_1 = (t_p)_3 = (t_p)_5 = 5ns$ and $(t_p)_2 = (t_p)_4 = 10ns$.

(ii) The Fourier transforms of the DQM time signals, taken along $t_5 = t_1$, for two sets of Euler angles: (a) $(\alpha_1, \beta_1, \gamma_1) = (0, 2\pi/3, 0), (\alpha_2, \beta_2, \gamma_2) = (0, \pi/6, 0)$ and (b) $(\alpha_1, \beta_1, \gamma_1) = (0, \pi/4, 0)$, $(\alpha_2, \beta_2, \gamma_2) = (0, \pi/6, 0)$ are shown in Fig. 9, as calculated for $d = 20$ MHz and $B_1 = 17.8\ G$. They are found to be highly sensitive to the relative orientations of the nitroxide radicals, showing that the DQM experiment is, indeed, sensitive to the structure of the coupled nitroxide biradical.

(iii) The effect of relaxation on the DQM signal in shown in Fig. 10, displaying the Fourier transform of the DQM signal without and with relaxation, calculated for the relaxation times $T_1 = 10\mu s$ (over the pathway $p = 0$), $T_2^S = 500$ ns (over the pathways $p = \pm 1$) and $T_2^D = 200$ ns (over the pathways $p = \pm 2$), using the stretching parameter β=*0.8,* $d = 40$ *MHz* and $B_1 = 17.8\ G$. As expected, the Pake doublets become broadened by relaxation. The relaxation times T_1 and T_2^S contribute to this broadening whereas T_2^D does not have any effect on the broadening of the peaks, since it operates over a constant time, reducing the intensity but not contributing to the broadening. Furthermore, T_2^S has more dominant contribution as compared to that of T_1 , as its value is shorter than T_1, since the relaxations factors are inversely proportional to the exponential of the relaxation time.

(iv) Figure 11 shows the simulation of the five-pulse DQM spectrum of the nitroxide biradical to fit the experimental data obtained by Saxena and Freed [20]. The simulations are carried out, using the same parameters as listed in [20], employing the numerical algorithm as given above in Sec. 4. The experimental data shown here is a profile of the maximum, i.e., that occurs for $t_5 = t_1$ of the three-dimensional experimental data (intensity versus t_5, t_1), reported in [20], The parameters used for the simulation are the same as that used in [20], which are specifically: B_1 =17.8 G; *d=12.3 MHz*, $T_2^S = 500ns$, $T_2^D = 300ns$; $(t_p)_1 = (t_p)_3 = (t_p)_5 = 5ns$ and $(t_p)_2 = (t_p)_4 = 10ns$. The other parameters are the same as those listed in Table I. The simulation shows a reasonably good agreement, within experimental errors, to the experiment [20].

(v) It is found from Figs. 2 and 8, showing the simulations of the Pake doublets for the two-pulse and five-pulse sequences, respectively, that the five-pulse DQM sequence produces much cleaner Pake doublets than does the two-pulse DQ sequence, as far as the side peaks are concerned.

8. Conclusions

The salient features of the present study are as follows.

(i) It is shown here from general considerations that a finite, rather than an infinite, pulse is needed, in conjunction with the dipolar interaction, to produce a non-zero coherence transfer in the transitions 0→2 and 2→-1 for both the two-pulse DQ and five-pulse DQM sequences.

(ii) The simulations show that the coherence transfer, $T_{0\rightarrow 2}$, as effected by a finite pulse in conjunction with the dipolar interaction, is found to increases as the amplitude of the irradiation field (B_1) decreases. Furthermore, it is maximum for those coupled nitroxides, whose dipolar axes are oriented symmetrically about $\pm 10^{\circ}$ away from the magic angle θ_0 ~ 54.74°, at which $(3cos^2\theta - 1) = 0$, for $0^{\circ} \leq \theta \leq 90^{\circ}$, being symmetric about $\theta = 90^{\circ}$ in the range $0^{\circ} \leq \theta \leq 180^{\circ}$, implying that these spins willl be preferentially pumped from $p = 0$ to $p = 2$ coherence state. ***This is a first-ever novel result, as far as orientational sensitivity is concerned,*** found with the help of extensive quantiative simulations for the first time. This orientational selectivity of the forbidden DQ signal occurs for d > 10 MHz up to a maximum value of B_1 that depends on d.. As for $20\,MHz \leq d \leq 40\,MHz$, it occurs for $B_1 \leq 3.0$ G for both two-pulse DQ and five-pulse DQM sequences. . It is noted that there is no orientational selectivity possible for $d \leq 10$ MHz.

(ii) The relaxation time over the double-quantum coherence pathway, T_2^D, can *only* be measured with the two-pulse DQ experiment. Knowing T_2^D, one can determine the relaxation time over the single-quantum coherence pathway, T_2^S, using the data for five-pulse DQM experiment. Furthermore, the DQM experiment enables the measurement of the spin-lattice relaxation time, T_1 . Thus, the DQ and DQM experiments play unique, important roles in the determination of various relaxation times.

(iii) A full derivation of the analytical expressions and a complete algorithm for the numerical simulations for two-pulse DQ and five-pulse DQM sequences, using a finite pulse, are given in this paper.

(iv) The Fourier transforms of the DQM signals depend upon the orientations of the two nitroxide magnetic dipoles as described by the respective sets of Euler angles. This can be exploied to study the structural geometry of the nitroxide biradical. This is a cutting-edge topic in the study of biomolecules.

(v) The Pake doublets occur at $\pm\frac{3}{2}d$ and $\pm d$ for the two-pulse DQ and five-pulse DQM signals in the polycrystalline averages, respectively, as calculated using Monte-Carlo simulations. The Pake doublets in polycrystalline averages for the two-pulse DQ and five-pulse DQM signals are direct measures of the dipolar interaction, from which the distance between the two nitroxide dipoles in

thebiradical used as spin probe, can be determined, being inversely proportional to the cube of the distance as $r = 10\big(51.9/d(MHz)\big)^{1/3}$, where d is the dipolar-coupling constant.

(vi) By comparing the Pake doublets, it is found that the five-pulse DQM sequence produces much cleaner Pake doublets than does the two-pulse DQ sequence.

(vii) For the purpose of distance measurement, it is shown here that one needs to perform only one-dimensional time-dependent experiments, i.e., involving only $t_2 = 2t_1$ for two-pulse DQ and $t_5 = t_1$ forfive-pulse DQM sequences.

(viii) The simulation of the five-pulse DQM signal calculated using the algorithm described here shows a good agreement with the experimental data.

Acknowledgments. We are grateful to the Natural Sciences and Engineering Council of Canada for partial financial support.

References

[1] R. Ernst, G. Bodenhausen, and A. Wokaun, Principles of Nuclear Magnetic Resonance in One and Two Dimensions, Clarendon Press, Oxford (1991).

[2] G. Wu, D. Rovnyank, B. Sun, and R. B. Griffin, “"High-resolution multiple quantum MAS NMR spectroscopy of half-integer quadrupolar nuclei”, *Chem. Phys. Lett*. **249**, 210 (1996).

[3] C. Fernandez and J. P. Amoureux, “2D multiquantum MAS-NMR spectroscopy of 27Al in aluminophosphate molecular sieves”, *Chem. Phys. Lett*. **242**, 449 (1995).

[4] A. Medek, J. S. Hardwood, and L. Frydman J. Am. Chem. Soc. **117**, 12779 (1995); J. P. Amoureux, C. Fernandez, and L. Frydman, *Chem. Phys. Lett*. **259**, 327 (1996).

[5] I. Solomon, “Multiple echoes in solids” *Phys. Rev.* **110**, 61 (1958).

[6] A. Abragam, *The Principles of Nuclear Magnetism,* Oxford University Press, New York, (1961) p. 245.

[7] S. Saxena and J. H. Freed, “Theory of double quantum two-dimensional electron spin resonance with application to distance measurements”, *J. Chem. Phys*, ***107***, 1317 (1997).

[8] S. K. Misra, P.P. Borbat and J. H. Freed, "Calculation of double-quantum-coherence two-dimensional spectra: distance measurements and orientational correlations", *Appl. Magn. Reson.* ***36***, 237 (2009).

[9] P.P, Borbat and J. H. Freed, "Double-quantum ESR and distance measurements", *Distance measurements in biological systems by EPR*, Springer, Boston, MA, pp. 383-459 (2002).

[10] P. P. Borbat and J. H. Freed, "Pros and cons of pulse dipolar ESR: DQC and DEER", *EPR newsletter*, 17 (2-3) (2007).

[11] A. M. Raitsimring and K. M. Salikhov, "Electron spin echo method as used to analyze the spatial distribution of paramagnetic centers". *Bull Magn Reson*, *7*(4), pp.184-217 (1985).

[12] A. D. Milov, K. M. Salikhov and M. D. Shirov, "Application of the double resonance method to electron spin echo in a study of the spatial distribution of paramagnetic centers in solids", *Sov. Phys. Solid State*, *23*, pp.565-569 (1981).

[13] K. M. Salikhov, S. A. Dzuba and A. M. Raitsimring, "The theory of electron spin-echo signal decay resulting from dipole-dipole interactions between paramagnetic centers in solids", *J. Magn. Reson*, *42*(2), pp.255-276 *(1969)*.

[14] A. D. Milov, K. M. Salikhov and Y. D. Tsvetkov, "Phase relaxation of hydrogen atoms stabilized in an amorphous matrix", *Phys. Solid State*, *15*(4), pp.802-806 (1973).

[15] A. D. Milov, Y. D. Tsvetkov, F. Formaggio, M. Crisma, C. Toniolo and J. Raap, "Self-assembling properties of membrane-modifying peptides studied by PELDOR and CW-ESR spectroscopies" *J. Am. Chem. Soc*, *122*(16), pp.3843-3848 (2000).

[16] A. D. Milov, Y. D. Tsvetkov, F. Formaggio, M. Crisma, C. Toniolo and J. Raap, "The secondary structure of a membrane-modifying peptide in a supramolecular assembly studied by PELDOR and CW-ESR spectroscopies", *J. Am. Chem. Soc*, *123*(16), pp.3784-3789 (2001).

[17] A. D. Milov, Y. D. Tsvetkov, F. Formaggio, S. Oancea, C. Toniolo and J. Raap, "Aggregation of spin labeled trichogin GA IV dimers: Distance distribution between spin labels in frozen solutions by PELDOR data", *J. Phys. Chem B*, *107*(49), pp.13719-13727 (2003).

[18] A. D. Milov, B. D. Naumov and Y. D. Tsvetkov, "The effect of microwave pulse duration on the distance distribution function between spin labels obtained by PELDOR data analysis", *Appl. Magn. Reson.*, *26*(4), p.587 (2004).

[19] A. D. Milov, and Y. D. Tsvetkov, "Double electron-electron resonance in electron spin echo: Conformations of spin-labeled poly-4-vinilpyridine in glassy solutions", *Appl. Magn. Reson*, *12*(4), pp.495-504 (1997).

[20] S. Saxena and J. H. Freed, "Double quantum two-dimensional Fourier transform electron spin resonance: Distance measurements", *Chem. Phys. Lett*, ***251***, 102 (1996).

[21] N. Stein, L. Mainali, J. S. Hyde and W. K. Subczynski, *Appl. Magn. Reason.*, *50*(7), pp.903-918 (2019).

[22] S. Pfenninger, W. E. Antholine, M. E. Barr, J. S. Hyde, P. M. Kroneck and W. G. Zumft, *Biophysical journal*, *69*(6), pp.2761-2769 (1995).

[23] S, K. Misra and H. R. Salahi, "Relaxation in Pulsed EPR: Thermal Fluctuation of Spin-Hamiltonian Parameters of an Electron-Nuclear Spin-Coupled System in a Malonic Acid Single Crystal in a Strong Harmonic-Oscillator Restoring Potential", *Appl. Magn. Reson*, pp.1-15 (2021).

[24] S. Lee, B. R. Patyal and J. H. Freed, "A two-dimensional Fourier transform electron-spin resonance (ESR) study of nuclear modulation and spin relaxation in irradiated malonic acid", *J. Chem Phys*, *98*(5), pp. 3665-3689 (1993).

[25] D. J. Schneider, J. H. Freed, "Spin Labeling: Theory and Application", Berliner, LJ., editor. Academic; New York: 1976. Chap. 2.

[26] The nitroxide static Hamiltonian H_0 missed the factor $\sqrt{2}$ in some matrix elements in [7].

[27] There was an error in the free-evolution propagator in [7], specifically, the expression (B.14): $e^{-iH_0t} = U^{\dagger}EU$ which should have been $e^{-iH_0t} = UEU^{\dagger}$. (This was, in fact, not a typo because Eq. (B.15) in [7] was consistent with Eq. (B.14).)

Appendix A. The static spin Hamiltonian for nitroxide biradical

In this appendix, the coefficients C, A and B of the static spin Hamiltonian for the two nitroxides of the biradical, given by Eq. (2.2), are defined; more details can be found in [7]. It can be expressed in terms of the irreducible spherical tensor operators (ISTO) as [7,8]

$$H_{0k} = \sum_{\mu_k,L,M} F^{L,M^*}_{\mu_k,l} A^{L,M}_{\mu_k,l} \;\; k \text{ (=1,2)} \tag{A.1}$$

where μ_k determines type of the interaction and takes two values: g_k and A_k for Zeeman and hyperfine interactions, respectively; k (=1,2) specifies the two nitroxides; L is the rank of the tensor; and M takes integer values between $-L$ and $+L$ for a given L. Here l stands for the *laboratory* frame, defined to be such that the z-axis is parallel to the static magnetic field [7]. In Eq. (A.1), $F^{L,M^*}_{\mu_k,l}$ are the standard ISTO components of the magnetic tensors of μ_k kind in the laboratory reference frame. These $F^{L,M^*}_{\mu_k,l}$s are conveniently defined in the magnetic g-frame of a nitroxide ($F^{L,M^*}_{\mu_k,g}$) and then transformed to the laboratory frame by two successive transformations: first, from the g-frame to the dipolar frame defined by its z-axis along the vector connecting the magnetic dipoles of the two nitroxides and then to the laboratory frame. The various components of $A^{L,M}_{\mu_k,l}$ and $F^{L,M}_{\mu_k,g}$ are listed in [25]. The high-field limit, wherein the contribution of the non-secular terms of $A^{L,M}_{\mu_k,l}$ (i.e., $S_{\pm}, S_{\pm}I_z, S_{\pm}I_{\pm}, S_{\pm}I_{\mp}$) is negligible, is used in this treatment [7]. Using the Wigner D-matrices $D^L_{m,m'}$, the transformed $F^{L,M^*}_{\mu_k,l}$ can then be expressed as

$$F^{L,M^*}_{\mu_k,l} = \sum_{m',m''} D^L_{m,m'}(\eta) D^L_{m',m''}(\lambda_k) F^{L,m''}_{\mu_k,g} \tag{A.2}$$

where $\eta = (0, \theta, \varphi)$ and $\lambda_k = (\alpha_k, \beta_k, \gamma_k)$ are the Euler angles defining the transformations from the laboratory frame to the dipolar frame and from the dipolar frame to the g_k frame, respectively. Inserting Eq. (A.2) into Eq. (A.1), the static Hamiltonian of two coupled nitroxides in the laboratory frame in the secular approximation, i.e., neglecting the non-secular terms, is

$$H_0 = \sum_{k=1,2} H_{0k} = \sum_{k=1,2} S_{zk}[C_k + A_k I_{zk} + B_k I_{+k} + B_k{}^* I_{-k}] \tag{A.3}$$

where the coefficients C_k, A_k, B_k are defined in the rotating frame as

$$C_k = \sqrt{\frac{2}{3}} \sum_{m'} D^2_{0,m'}(\eta_k) K_{g_k,m'}(\lambda_k) \tag{A.4}$$

$$A_k = \sqrt{\frac{2}{3}} \sum_{m'} D^2_{0,m'}(\eta_k) K_{A_k,m'}(\lambda_k) + \frac{g_e \beta_e}{3\hbar}\left(A_{xx} + A_{yy} + A_{zz}\right) \tag{A.5}$$

$$B_k = \frac{1}{2} \sum_{m'} D^2_{1,m'}(\eta_k) K_{A_k,m'}(\lambda_k) \tag{A.6}$$

It is noted that the isotropic part of the Zeeman term is put equal to zero in the rotating frame and the Zeeman term, as given by Eq. (A.4), is the resonant offset term as calculated here quantitively. The $K_{\mu_i,m'}$ terms in Eqs. (A.4)-(A.6), which contain the transformation from the magnetic frame to the dipolar frame, are defined as

$$K_{\mu_i,m'}(\lambda_i) = \left[D^2_{m',2}(\lambda_i) + D^2_{m',-2}(\lambda_i)\right] F^{2,2}_{\mu_i,g} + D^2_{m',0}(\lambda_i) F^{2,0}_{\mu_i,g} \tag{A.7}$$

Appendix B. Matrix representation, eigenvalues, and eigenvectors

In this Appendix, the eigenvalues and the eigenvectors of the static spin Hamiltonian, given by Eq. (2.1):

$$H_0 = H_{01} + H_{02} + H_{12} \tag{2.1}$$

of the two coupled nitroxides including the dipolar and exchange interactions are given. For matrix representation of the static Hamiltonian, the magnetic basis, defined in the direct product of the electron spin basis eigenvectors $M_S = |+\rangle$ and $|-\rangle$ and the nuclear spin basis eigenvectors, m_I= $|-1\rangle, |0\rangle$ and $|1\rangle$, are used. In this basis, the matrix representation of, for example, Eq. (A.3),

$$H_0 = \sum_{k=1,2} H_{0k} = \sum_{k=1,2} S_{zk}[C_k + A_k I_{zk} + B_k I_{+k} + B_k{}^* I_{-k}] \tag{A.3}$$

for one of the nitroxide biradicals, can be expressed as [26]

$$H_{01} = \begin{pmatrix} \frac{1}{2}(A_1 + C_1) & \frac{B_1}{\sqrt{2}} & 0 & 0 & 0 & 0 \\ \frac{B_1}{\sqrt{2}} & \frac{C_1}{2} & \frac{B_1}{\sqrt{2}} & 0 & 0 & 0 \\ 0 & \frac{B_1}{\sqrt{2}} & \frac{1}{2}(C_1 - A_1) & 0 & 0 & 0 \\ 0 & 0 & 0 & \frac{-1}{2}(A_1 + C_1) & -\frac{B_1}{\sqrt{2}} & 0 \\ 0 & 0 & 0 & -\frac{B_1}{\sqrt{2}} & -\frac{C_1}{2} & -\frac{B_1}{\sqrt{2}} \\ 0 & 0 & 0 & 0 & -\frac{B_1}{\sqrt{2}} & \frac{1}{2}(A_1 - C_1) \end{pmatrix} \quad \text{(B.1)}$$

The Hamiltonian in Eq. (B.1) is diagonalized by the unitary transformation $E_1 = {T^{(1)}}^{\dagger} H_{01} T^{(1)}$, where $T^{(1)}$ is:

$$T^{(1)} = \begin{pmatrix} T_{\alpha}^{(1)} & 0 \\ 0 & T_{\alpha}^{(1)} \end{pmatrix}. \quad \text{(B.2)}$$

Here $T_{\alpha}^{(1)}$ is a 3×3 matrix given by using the basis vectors $\left(|\psi_{-1}{}^{(1)}\rangle, |\psi_{0}{}^{(1)}\rangle, \psi_{1}{}^{(1)}\rangle\right)$, as

$$T_{\alpha}^{(1)} = \begin{pmatrix} \frac{A_1(A_1 + \omega) + 2|B_1|^2}{\omega_+} & -\frac{|B_1|}{\sqrt{2}\omega} & \frac{-A_1\omega + A_1^2 + 2|B_1|^2}{\omega_-} \\ \frac{\sqrt{2}(A_1 + \omega)|B_1|}{\omega_+} & \frac{A_1}{\omega} & \frac{\sqrt{2}(A_1 - \omega)|B_1|}{\omega_-} \\ \frac{2|B_1|^2}{\omega_+} & \frac{|B_1|}{\sqrt{2}\omega} & \frac{2|B_1|^2}{\omega_-} \end{pmatrix} \quad \text{(B.3)}$$

where,

$$\omega = \sqrt{A_1^2 + 4|B_1|^2}$$
$$\omega_+ = \sqrt{2(A_1+\omega)(3A_1+\omega)|B_1|^2 + A_1^2(A_1+\omega)^2 + 8|B_1|^4} \quad \text{(B.3a)}$$
$$\omega_- = \sqrt{2(\omega-A_1)(\omega-3A_1)|B_1|^2 + A_1^2(\omega-A_1)^2 + 8|B_1|^4}$$

Similar results for diagonalization of the spin Hamiltonian H_{02} for the second nitroxide are obtained by $A_1 \rightarrow A_2$ and $B_1 \rightarrow B_2$.

The spin Hamiltonian of the coupled nitroxides system in Eq. (A.3) with the dimension of the Hilbert space $(2S_1+1)(2S_2+1)(2I_1+1)(2I_2+1)X(2S_1+1)(2S_2+1)(2I_1+1)(2I_2+1) = 36 \times 36$ can be split into sixteen 9×9 blocks, of which only six blocks have non-zero elements, as shown in matrix (B.5) below,. These are: (1,1), (2,2), (2,3), (3,2), (3,3) and (4,4). Each such block, H_{ij}, is diagonalized by the unitary transformation $U^\dagger H_{ij} U$,where U is constructed from the direct product of spin basis eigenvectors of the two coupled nuclei, as

$$T_\alpha^{(1)} \otimes T_\alpha^{(2)} = \left|\psi_j{}^{(1)}; \psi_k{}^{(2)}\right\rangle \quad \text{(B.4)}$$

where $j,k = -1,0,1$. Using the eigenvectors, given by Eq (B.4), the static Hamiltonian matrix of the coupled nitroxides system is expressed as

$$H_0 = \begin{pmatrix} [[H_{11}]] & [[0]] & [[0]] & [[0]] \\ [[0]] & [[H_{22}]] & [[H_{23}]] & [[0]] \\ [[0]] & [[H_{32}]] & [[H_{33}]] & [[0]] \\ [[0]] & [[0]] & [[0]] & [[H_{44}]] \end{pmatrix} \quad \text{(B.5)}$$

where the double square bracket [[]] indicates a 9×9 diagonal matrix. In Eq. (B.5), the blocks $[[H_{32}]] = [[H_{23}]]$ (they consist of real matrix elements) are non-zero due to the dipolar interaction between the two nitroxide radicals. Each matrix element in Eq. (B.5), indicated by double square brackets, is described by the indices l,m in the direct-product space, which correspond to the combinations of $j,k,j',k' = -1,0,1$ as follows: $l = 3j+k+5, m = 3j'+k'+5$, so that l,m=1, 2, ….,9. These are given, in terms of *j,* k (=*j'*, k') by

$$(H_{11})_{lm} = \frac{1}{2}[C_1 + C_2 + (A_1^2 + 4|B_1|^2 j)^{1/2} j + (A_2^2 + 4|B_2|^2 k)^{1/2} k] + \frac{d}{4}(3cos^2\theta - 1)\delta_{lm},$$

$$(H_{22})_{lm} = \frac{1}{2}[C_1 - C_2 + (A_1^2 + 4|B_1|^2 j)^{1/2} j - (A_2^2 + 4|B_2|^2 k)^{1/2} k] - \frac{d}{4}(3cos^2\theta - 1)\delta_{lm},$$

$$(H_{23})_{lm} = (H_{32})_{lm} = -\frac{d}{4}(3cos^2\theta - 1)\delta_{lm},$$

$$(H_{33})_{lm} = \frac{1}{2}[-C_1 + C_2 - (A_1^2 + 4|B_1|^2 j)^{1/2} j + (A_2^2 + 4|B_2|^2 k)^{1/2} k] - \frac{d}{4}(3cos^2\theta - 1)\delta_{lm},$$

$$(H_{44})_{lm} = -\frac{1}{2}[C_1 + C_2 + (A_1^2 + 4|B_1|^2 j)^{1/2} j + (A_2^2 + 4|B_2|^2 j)^{1/2} k] + \frac{d}{4}(3cos^2\theta - 1)\delta_{lm} \quad \text{(B.6)}$$

The static Hamiltonian H_0, represented in matrix form in Eq. (B.5), can be diagonalized by a unitary transformation S as $E = S^{\dagger} H_0 S$, where S is

$$S = \begin{pmatrix} [[1]] & [[0]] & [[0]] & [[0]] \\ [[0]] & [[\xi]] & [[\zeta]] & [0]] \\ [[0]] & [[-\zeta]] & [[\xi]] & [0]] \\ [[0]] & [[0]] & [[0]] & [[1]] \end{pmatrix}, \quad \text{(B.7)}$$

In Eq. (B.7), $i = 1,2,\ldots,9$ will be used to specify the matrix elements in the hyperfine subspace, indicated by the matrices $[[\ \ ]]$, so that $[[\xi]]$ and $[[\zeta]]$ are 9×9 diagonal matrices, with the ith diagonal elements being $\xi_{ii} = \cos(\Xi_i)$ and $\zeta_{ii} = \sin(\Xi_i)$, respectively. The elements $\Xi_i$can be determined from

$$\tan(2\Xi_i) = \frac{2(H_{23})_{ii}}{(H_{33})_{ii} - (H_{22})_{ii}} \quad \text{(B.8)}$$

. The eigenvalue matrix of the coupled-nitroxides system, expressed as

$$E = \begin{pmatrix} [[E_1]] & [[0]] & [[0]] & [[0]] \\ [[0]] & [[E_2]] & [[0]] & [[0]] \\ [[0]] & [[0]] & [[E_3]] & [[0]] \\ [[0]] & [[0]] & [[0]] & [[E_4]] \end{pmatrix} \quad \text{(B.9)}$$

where the lth $(l = 1,\ldots,9)$ diagonal elements of the various $[[E_n]]$, $(n = 1,2,3,4)$are given by

$[[E_1]]_{ll} = (H_{11})_{ll}$,

$$[[E_2]]_{ll} = -\frac{d}{4}(3cos^2\theta - 1) - \left[\left(\frac{d}{4}(3cos^2\theta - 1)\right)^2 + \frac{1}{4}\left(C_1 - C_2 + (A_1^2 + 4|B_1|^2 j)^{1/2} j - (A_2^2 + 4|B_2|^2 k)^{1/2} k^2 \right)^2\right],$$

$$[[E_3]]_{ll} = -\frac{d}{4}(3cos^2\theta - 1) + \left[\left(\frac{d}{4}(3cos^2\theta - 1)\right)^2 + \frac{1}{4}\left(C_1 - C_2 + (A_1^2 + 4|B_1|^2 j)^{1/2} j - (A_2^2 + 4|B_2|^2 k)^{1/2} k^2 \right)^2\right],$$

$$[[E_4]]_{ll} = (H_{44})_{ll} \tag{B.10}$$

In Eq. (B.10), the various l ($l = 1, \ldots, 9$) indices are calculated from the j, k indices by the relation $l = 3j + k + 5$ with $j, k = -1,0,1$.

To calculate the density matrix under free evolution, described by Eq. (2.9), one first needs to calculate $e^{-IH_0 t}$ [27] This can be achieved by transforming the matrix, expressed as the exponential of the eigenvalues of $H_0$with the unitary transformation S, as

$$e^{-IH_0 t} = S\, e^{-IEt} S^{\dagger}$$

$$= \begin{pmatrix} [[e^{-i\mathrm{E}_1 t}]] & [[0]] & [[0]] & [[0]] \\ [[0]] & e^{-i[[\mathrm{E}_2]]t}[[\xi^2]] + e^{-i[[\mathrm{E}_3]]t}[[\zeta^2]] & [[\zeta]]\,[[\xi]]\left(e^{-i[[\mathrm{E}_2]]t} - e^{-i[[\mathrm{E}_3]]t}\right) & [[0]] \\ [[0]] & [[\zeta]]\,[[\xi]]\left(e^{-i[[\mathrm{E}_2]]t} - e^{-i[[\mathrm{E}_3]]t}\right) & e^{-i[[\mathrm{E}_2]]t}[[\xi^2]] + e^{-i[[\mathrm{E}_3]]t}[[\zeta^2]] & [[0]] \\ [[0]] & [[0]] & [[0]] & \left[\left[e^{-i\mathrm{E}_4 t}\right]\right] \end{pmatrix} \tag{B.11}$$

In Eq. (B.11), the terms like $[[e^{-i\mathrm{E}_1 t}]]$=$diag\{e^{-i[[E_1]]_{ll} t}\}; l = 1,2, \ldots, 9$ and $[[\xi]] = diag\{\cos(\Xi_l)\}; l = 1,2, \ldots, 9$, where the terms on the right-hand sides are defined in Eqs. (B.10) and (B.8), respectively.

Appendix C. Projection operators for the various coherence pathways

The projection operators to project the density matrix on to the coherence pathway of interest after the application of a pulse are listed in this appendix for the coherence pathways $p = \pm 1$, $p = \pm 2$ and $p = 0$ as used in the calculation of DQ and DQM signals and discussed in Sec. 3. After the application of a projection operator, only those 9×9 hyperfine blocks of the density matrix which correspond to the non-zero elements of the projection operator are retained in the 4x4 electronic-spin space, putting all the other elements of the density matrix equal to zero.

Coherent pathway	Matrix
$p = +1$	$\begin{pmatrix} 0 & 1 & 1 & 0 \\ 0 & 0 & 0 & 1 \\ 0 & 0 & 0 & 1 \\ 0 & 0 & 0 & 0 \end{pmatrix}$
$p = -1$	$\begin{pmatrix} 0 & 0 & 0 & 0 \\ 1 & 0 & 0 & 0 \\ 1 & 0 & 0 & 0 \\ 0 & 1 & 1 & 0 \end{pmatrix}$
$p = 0$	$\begin{pmatrix} 1 & 0 & 0 & 0 \\ 0 & 1 & 1 & 0 \\ 0 & 1 & 1 & 0 \\ 0 & 0 & 0 & 1 \end{pmatrix}$
$p = +2$	$\begin{pmatrix} 0 & 0 & 0 & 1 \\ 0 & 0 & 0 & 0 \\ 0 & 0 & 0 & 0 \\ 0 & 0 & 0 & 0 \end{pmatrix}$
$p = -2$	$\begin{pmatrix} 0 & 0 & 0 & 0 \\ 0 & 0 & 0 & 0 \\ 0 & 0 & 0 & 0 \\ 1 & 0 & 0 & 0 \end{pmatrix}$

Appendix E. Five-pulse DQM signal

In this Appendix, the $M_i, i = 1, \ldots, 4$ terms used in the analytical expression of five-pulse DQM signal in Eq. (3.20) are provided. The $P_{ij}^{(2)}$ terms used here are the matrix elements of the propagation operator as defined by Eq. (2.13).

$$\begin{aligned} M_1 &= P_{12}^{(2)} + P_{13}^{(2)} \\ M_2 &= P_{42}^{(2)} + P_{43}^{(2)} \\ M_3 &= P_{22}^{(2)} + P_{23}^{(2)} \\ M_4 &= P_{32}^{(2)} + P_{33}^{(2)} \end{aligned} \tag{E.1}$$

Appendix D. Flowchart for the calculation of the of 2-pulse DQ or 5-pulse DQM signal

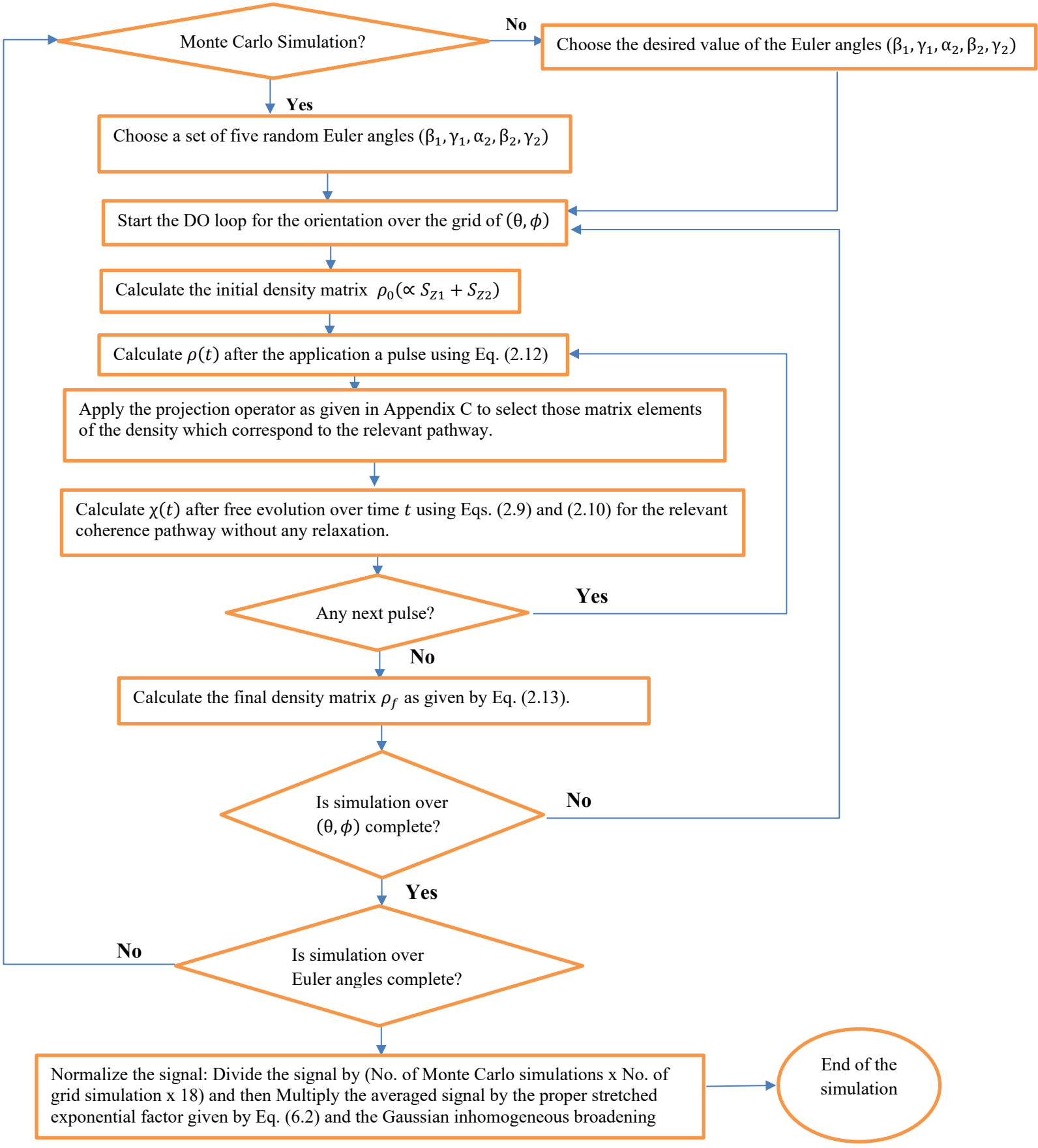

Table I. The free evolution terms for $p = 0$, $p = +1$ and $p = +2$ used in the analytical expressions in Sec. 3. The superscripts on $S_i(t)$ indicates the coherence pathway. The free evolution terms corresponding to $p = -1$ and $p = -2$ are the complex conjugate of those for $p = +1$ and $p = +2$, respectively.

$S_1^{(0)}(t)$	$-\frac{1}{4}\sin^2[[2\Xi]]\left([[e^{it\omega_{23}}]] + [[e^{it\omega_{32}}]] - [[2]]\right)$
$S_2^{(0)}(t)$	$-\frac{1}{4}sin[[4\Xi]] + sin[[\Xi]]\cos^3[[\Xi]][[e^{it\omega_{23}}]] - \cos[[\Xi]]\sin^3[[\Xi]][[e^{it\omega_{32}}]]$
$S_3^{(0)}(t)$	$\frac{1}{4}\left(\cos[[4\Xi]] + \sin^2[[2\Xi]]\left([[e^{it\omega_{23}}]] + [[e^{it\omega_{32}}]]\right) + [[3]]\right)$
$S_4^{(0)}(t)$	$2\sin^2[[\Xi]]\cos^2[[\Xi]] + \sin^4[[\Xi]][[e^{it\omega_{32}}]] + \cos^4[[\Xi]][[e^{it\omega_{23}}]]$
$S_1^{(+1)}(t)$	$[[e^{-it\omega_{13}}]]\sin^2[[\Xi]] + [[e^{-it\omega_{12}}]]\cos^2[[\Xi]]$
$S_2^{(+1)}(t)$	$([[e^{-it\omega_{13}}]] - [[e^{-it\omega_{12}}]])\sin[[\Xi]]\cos[[\Xi]]$
$S_3^{(+1)}(t)$	$[[e^{-it\omega_{34}}]]\sin^2[[\Xi]] + [[e^{-it\omega_{24}}]]\cos^2[[\Xi]]$
$S_4^{(+1)}(t)$	$\left([[e^{-it\omega_{34}}]] - [[e^{-it\omega_{24}}]]\right)\sin[[\Xi]]\cos[[\Xi]]$
$S_5^{(+1)}(t)$	$[[e^{-it\omega_{12}}]]\sin^2[[\Xi]] + [[e^{-it\omega_{13}}]]\cos^2[[\Xi]]$
$S_6^{(+1)}(t)$	$[[e^{-it\omega_{24}}]]\sin^2[[\Xi]] + [[e^{-it\omega_{34}}]]\cos^2[[\Xi]]$
$S_1^{(+2)}(t)$	$[[e^{-it_1\omega_{14}}]]$

Table II. The values of the parameters used in the simulations of the pulsed-EPR DQ and DQM signals of the coupled nitroxides.

Parameter	value
Static magnetic field (B_0)	$3{,}300G$
Microwave frequency	17.3 GHz
Exchange constant (J)	*0* MHz
Gaussian inhomogeneous broadening parameter (Δ_G)	5 MHz
Double quantum time ($t_3 = t_4 = t_{DQ}^{DQM}$)	50 ns
Stretched exponential parameter (β)	0.8
g-matrix $\tilde{\boldsymbol{g}} = (\boldsymbol{g_{xx}}, \boldsymbol{g_{yy}}, \boldsymbol{g_{zz}})$	(2.0086,2.0066,2.0032)
Hyperfine matrix $\tilde{\boldsymbol{A}} = (\boldsymbol{A_{xx}}, \boldsymbol{A_{yy}}, \boldsymbol{A_{zz}})$	(6.0 MHz,6.0 MHz,35.0 MHz)
Spin-lattice relaxation time (T_1)	10 μs

Figures

Fig. 1

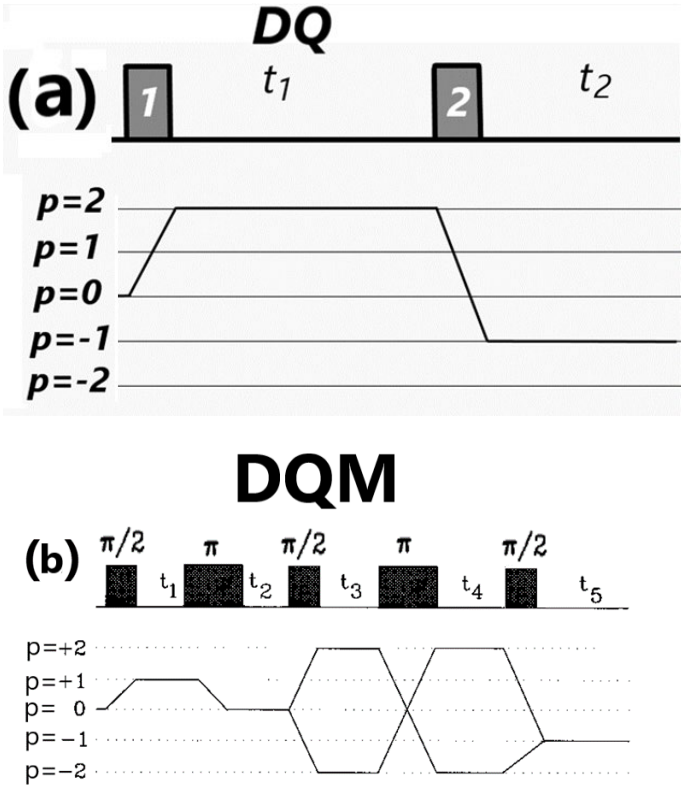

Fig. 1 The pulse schemes and the relevant coherence pathways for (a) two-pulse DQ, where 1 and 2 are finite pulses of any duration; (b) five-pulse DQM. For the two-pulse DQ sequence, the tip angle is determined as $\beta = \gamma_e B_1 t_p$ where B_1 is the amplitude of the microwave field and t_p is the duration of the pulse. For five-pulse DQM, finite, with the tip angle being almost $\pi/2$, or π, are used as shown. Here p is the coherence order, which represents transverse magnetization, corresponding to the spins rotating in a plane perpendicular to the external field.

Fig. 2.

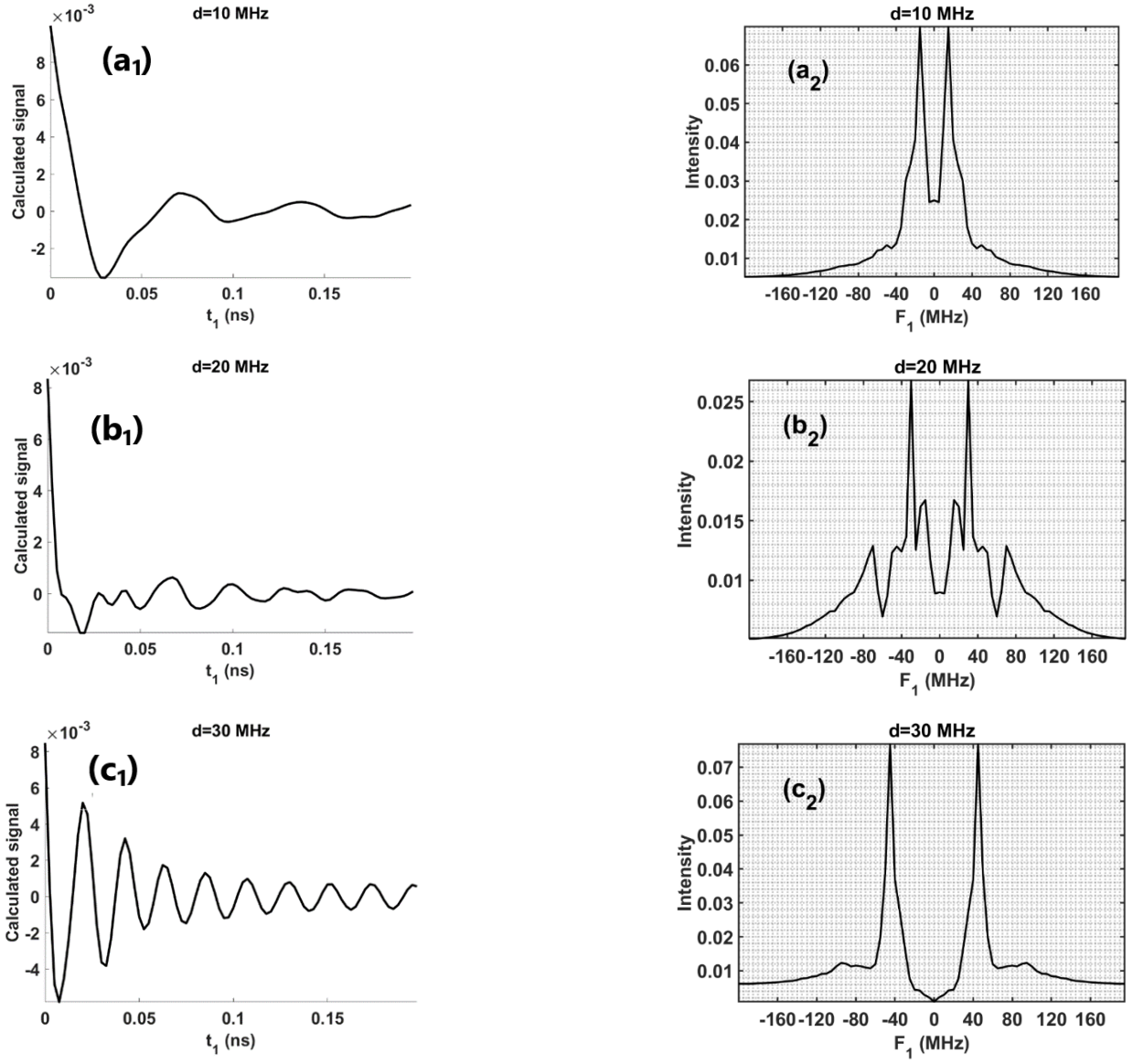

Fig. 2 Dependence of the two-pulse DQ signal on dipolar-coupling constant for a polycrystalline sample, averaged over twenty Monte-Carlo orientations of the nitroxide dipoles: left (a_1, b_1, c_1) time domain DQ signals for $t_2 = 2t_1$ and right (a_2, b_2, c_2) their Fourier transforms (Pake doublets) for three different values of the dipolar-coupling constant $d = 10, 20. 30$ MHz. The magnitude of the radiation microwave field $B_1 = 10G$ and the duration of the finite pulses $t_p = 80$ ns are used for all simulations. All other parameters used for the simulations are listed in Table II. Relaxation is not considered in these simulations. All Pake doublets appear at $\pm 3d/2$, in agreement with those calculated analytically as given by Eq. (3.18).

Fig. 3

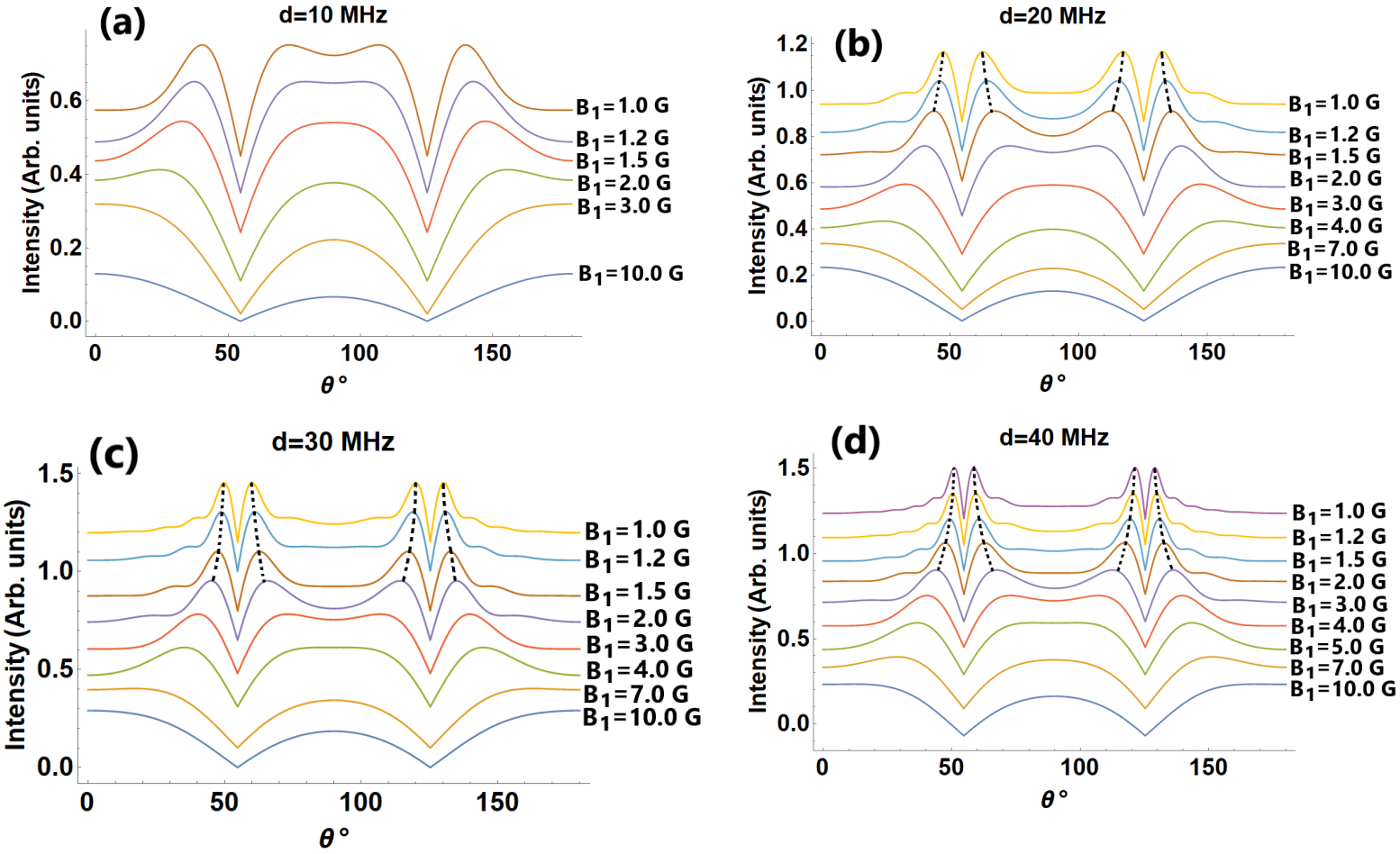

Fig. 3. The coherence transfer $T_{0\to 2}$, as calculated using Eq. (3.12), plotted as function of θ for different values of the amplitude of the irradiation field, B_1, indicated next to each plot for (a) $d =$ 10 MHz, (b) $d = 20$ MHz, (c) $d = 30$ MHz and (d) $d = 40$ MHz. The duration of the pulse t_p in each case is chosen consistent with a nominal $\pi/2$ pulse for each B_1 . Regardless of the values of d and B_1, the coherence transfer is zero at $\theta = 54.74^\circ$ and at $\theta = 125.26^\circ$, i.e., the values which make $(3cos^2(\theta) - 1) = 0$. The orientational selectivity, related to the sharpness of the peaks, occurs at lower values of B_1 for each d value, as indicated by thick dotted lines in each figure. It is noted that there is no such value possible for $d \leq 10$ MHz.

Fig. 4

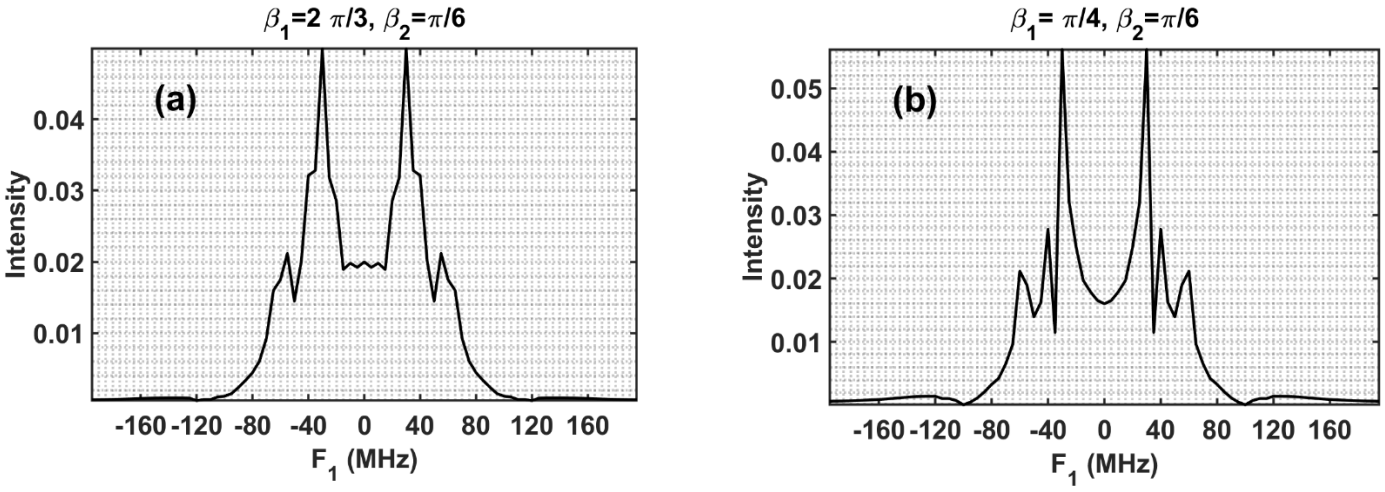

Fig. 4. Orientational dependence of the two-pulse DQ signal. The effect of the orientation of the nitroxide radicals on the DQ Fourier transform for a polycrystalline sample is shown in this figure. The Fourier transform as a function of t_1 of the one-dimensional time-domain signal along $t_2 = 2t_1$ for the orientations of the two nitroxide dipoles: (a) $(\alpha_1, \beta_1, \gamma_1) = (0,2\pi/3,0), (\alpha_2, \beta_2, \gamma_2) = (0, \pi/6,0)$ and (b) $(\alpha_1, \beta_1, \gamma_1) = (0, \pi/4,0), (\alpha_2, \beta_2, \gamma_2) = (0, \pi/6,0)$. The dipolar coupling constant $d = 20$ MHz and the amplitude of the irradiation microwave field $B_1 = 10.0\ G$ are used in the simulations. The values of all other parameters used in the simulations are listed in Table II. The Fourier transforms of the DQ signal are quite sensitive to the relative orientations of the nitroxide biradicals, making the DQ experiment feasible for structural studies.

Fig. 5

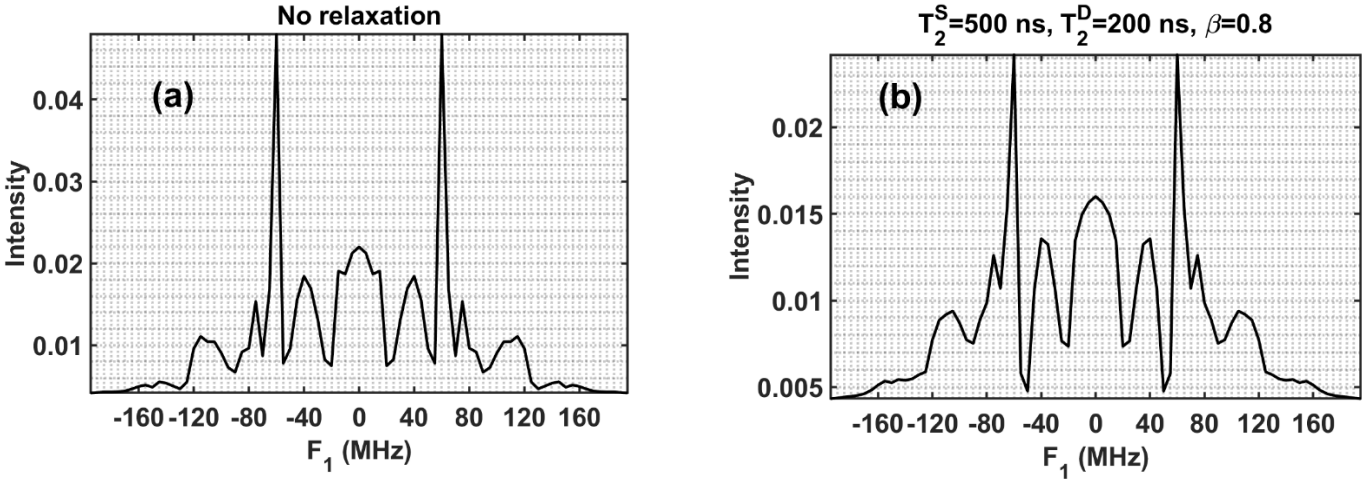

Fig. 5. Effect of relaxation on the DQ signal for a polycrystalline sample, averaged over twenty Monte-Carlo orientations of the nitroxide dipoles. The Fourier transform as a function of t_1 of the time domain DQ signal at $t_2 = 2t_1$ for: (left) without taking relaxation into account and (right) with relaxation included for $T_2^S = 500\,ns$ and $T_2^D = 200\,ns$ using the stretching parameter $\beta = 0.8$. The dipolar coupling constant $d = 40$ MHz and the amplitude of the irradiation microwave field $B_1 = 10.0\,G$ are used in these simulations. The values of all the other parameters used in the simulations are listed in Table II. Due to relaxation, the peaks are broadened, and the intensity of the calculated Fourier transform of the DQ signal is reduced by a factor of two.

Fig. 6

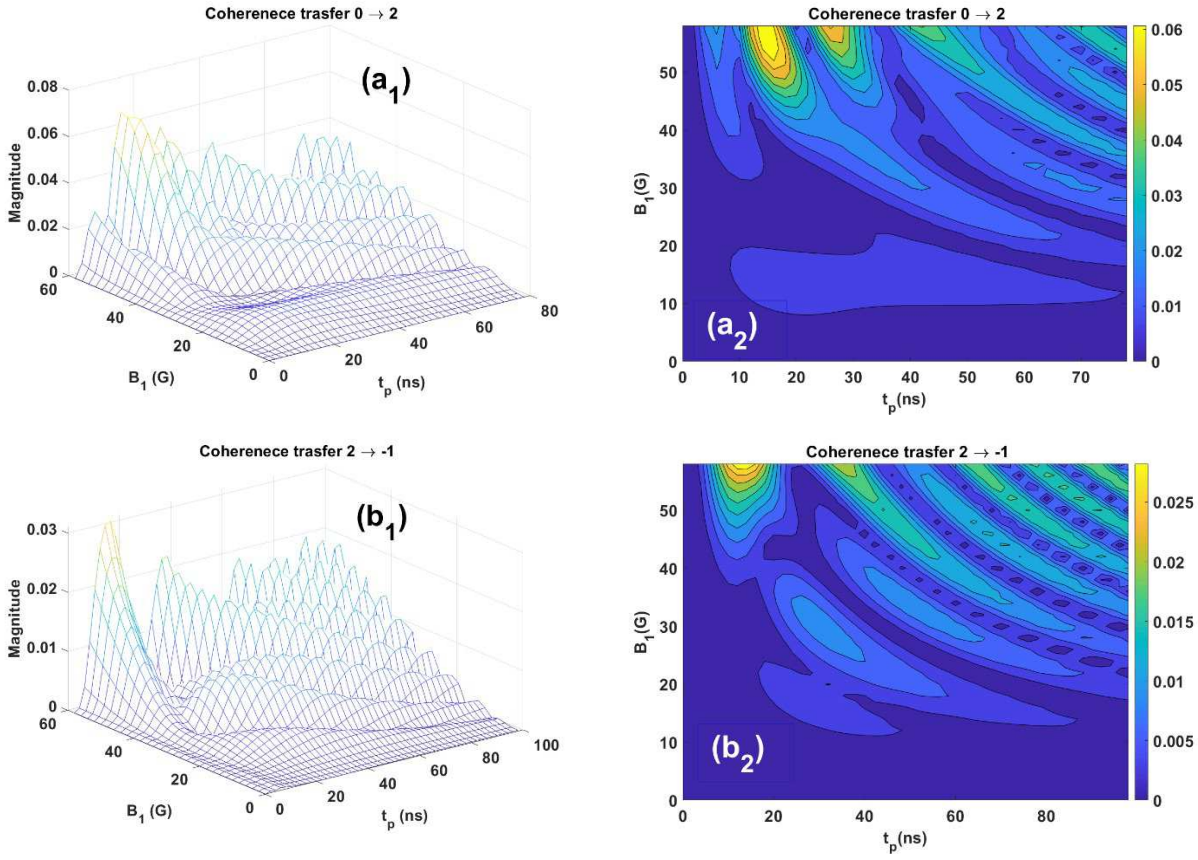

Fig. 6 Two-pulse DQ coherence transfers for a polycrystalline sample, averaged over twenty Monte-Carlo orientations of the nitroxide dipoles**:** (left) absolute values and (right) their contour plots of (top) 0 → 2 and (bottom) 2 →-1 coherence transfers), as functions of the intensity of the microwave magnetic field B_1 and the duration of the pulses, t_p (the same duration was chosen for the two pulses) for the dipolar coupling constant $d = 10$ MHz. All the parameters used for simulations are the same as those mentioned in the caption of Fig. 2. It is seen from these simulations that for the coherence transfers achieved with $B_1 = 60\ G$ and $t_p = 80$ ns of ~ 0.10 or each of the $T_{0\to2}$and $T_{2\to-1}$ transitions between the coherent pathways are reasonably large, making these B_1 and t_p values feasible for experimental purposes.

Fig. 7

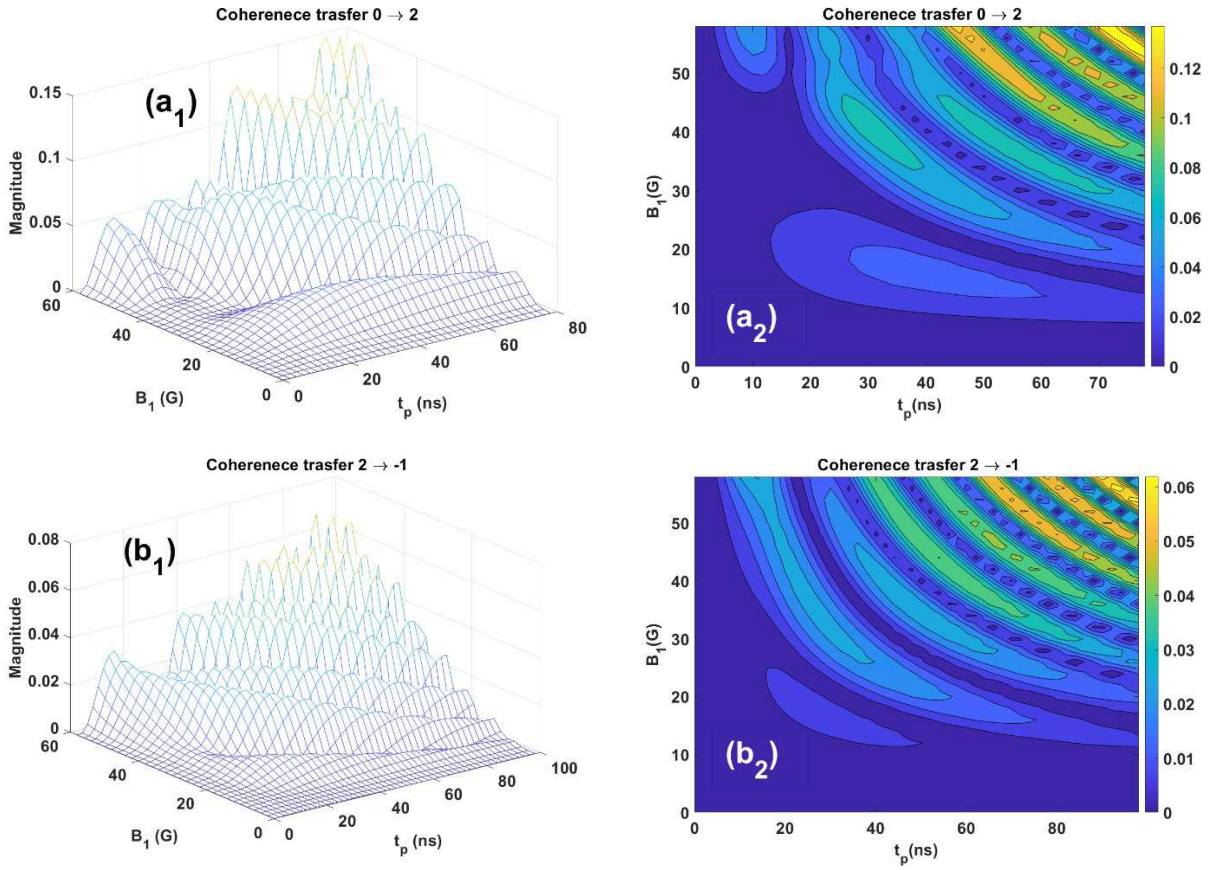

Fig. 7 The same details as those for Fig. except that here the simulations are for the dipolar-coupling constant $d = 30\ MHz$

Fig. 8

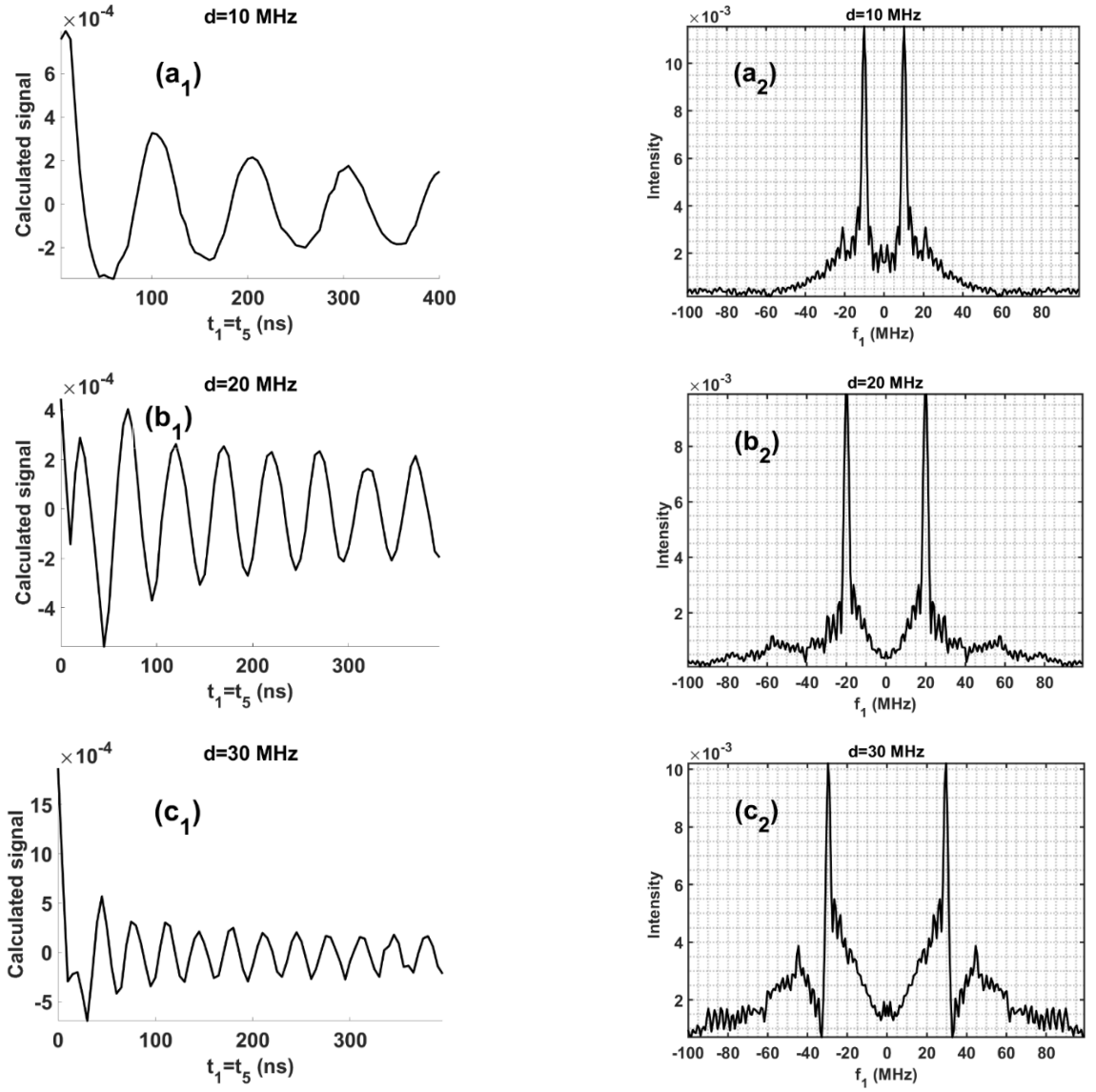

Fig. 8. Dependence of the five-pulse DQM signal on dipolar-coupling constant for a polycrystalline sample, averaged over twenty Monte-Carlo orientations of the nitroxide dipoles: left (a_1, b_1, c_1) time domain DQ signals for $t_5 = t_1$ and right (a_2, b_2, c_2) their Fourier transforms (Pake doublets) for three different values of the dipolar-coupling constant $d = 10, 20.30$ MHz. The magnitude of the radiation microwave field $B_1 = 17.8G$ and the duration of the finite pulses $(t_p)_1 = (t_p)_3 = (t_p)_5 = 5ns$ and $(t_p)_2 = (t_p)_4 = 10ns$ ns are used for all simulations. All other parameters used for the simulations are listed in Table II. Relaxation is not considered in these simulations. All Pake doublets appear at $\pm d$, in agreement with those calculated analytically as given by Eq. (3.20).

Fig. 9

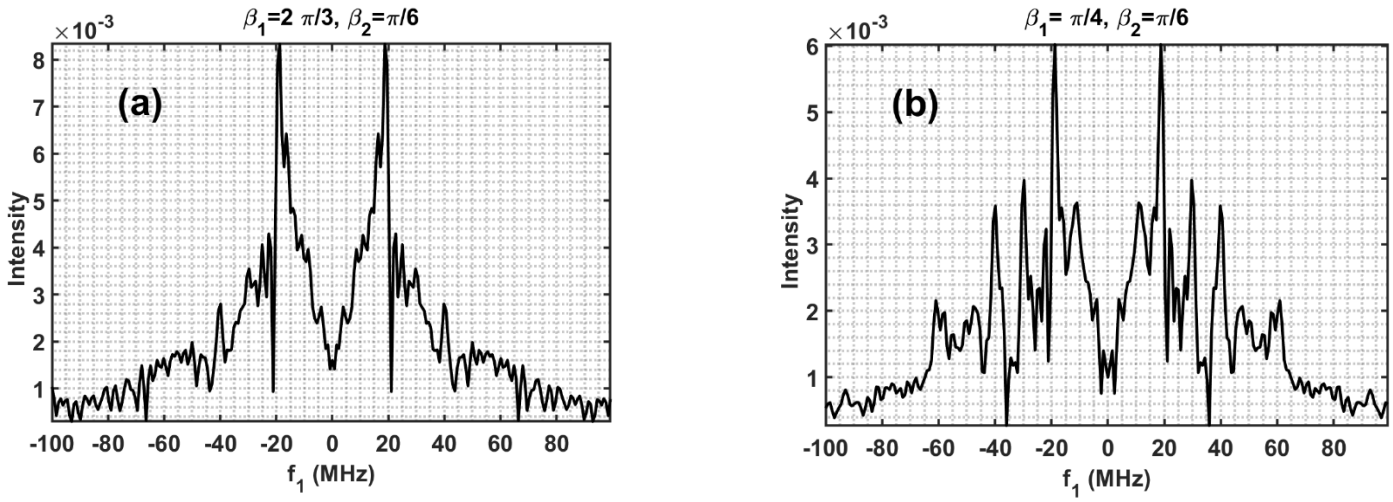

Fig. 9. Orientational dependence of the five-pulse DQM signal. The effect of the orientation of the nitroxide radicals on the DQM Fourier transform for a polycrystalline sample is shown in this figure. The Fourier transform as a function of t_1 of the one-dimensional time-domain signal along $t_2 = 2t_1$ for the orientations of the two nitroxide dipoles: (a) $(\alpha_1, \beta_1, \gamma_1) = (0, 2\pi/3, 0), (\alpha_2, \beta_2, \gamma_2) = (0, \pi/6, 0)$ and (b) $(\alpha_1, \beta_1, \gamma_1) = (0, \pi/4, 0), (\alpha_2, \beta_2, \gamma_2) = (0, \pi/6, 0)$. The dipolar coupling constant $d = 20$ MHz and the amplitude of the irradiation microwave field $B_1 = 17.8\ G$ are used in the simulations. The values of all other parameters used in the simulations are listed in Table II. A comparison of Figs. (a) and (b) shows that the Fourier transforms of the DQM signal are quite sensitive to the relative orientations of the nitroxide biradicals, making the DQM experiment feasible for structural studies.

Fig. 10

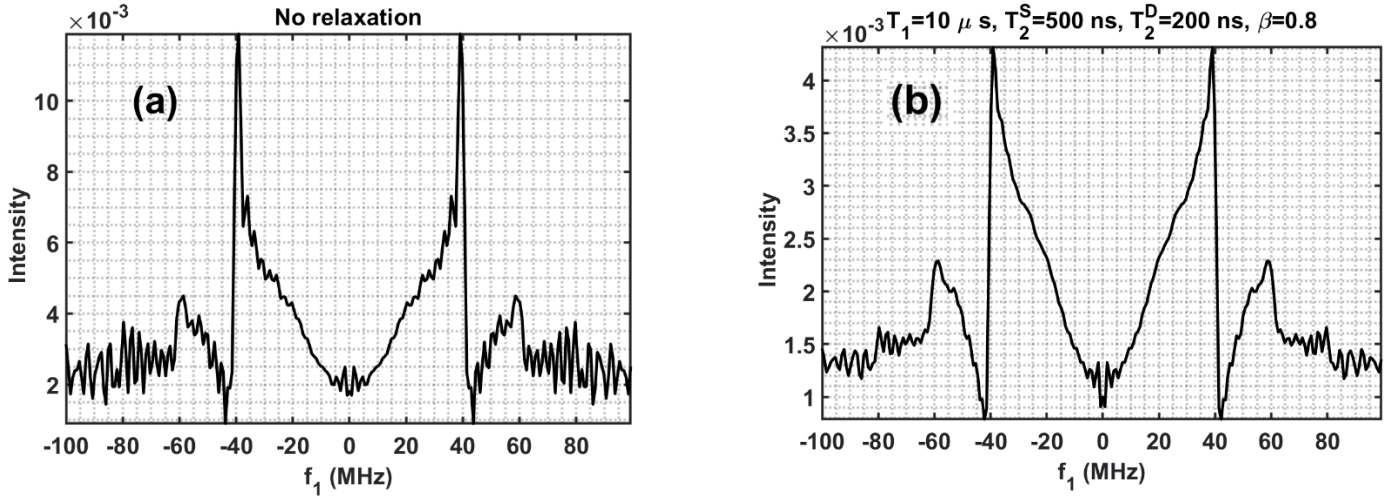

Fig. 10. Effect of relaxation on the DQM signal for a polycrystalline sample, averaged over twenty Monte-Carlo orientations of the nitroxide dipoles. The Fourier transform as a function of t_1 of the time domain DQM signal at $t_5 = t_1$ for: (left) without taking relaxation into account and (right) with relaxation included for $T_2^S = 500\,ns$ and $T_2^D = 200\,ns$ using the stretching parameter $\beta = 0.8$. The dipolar coupling constant $d = 40$ MHz and the amplitude of the irradiation microwave field $B_1 = 17.8\,G$ are used in these simulations. The values of all the other parameters used in the simulations are listed in Table II. Due to relaxation, the peaks are broadened, and the intensity of the calculated Fourier transform of the DQM signal is reduced by a factor of three.

Fig. 11

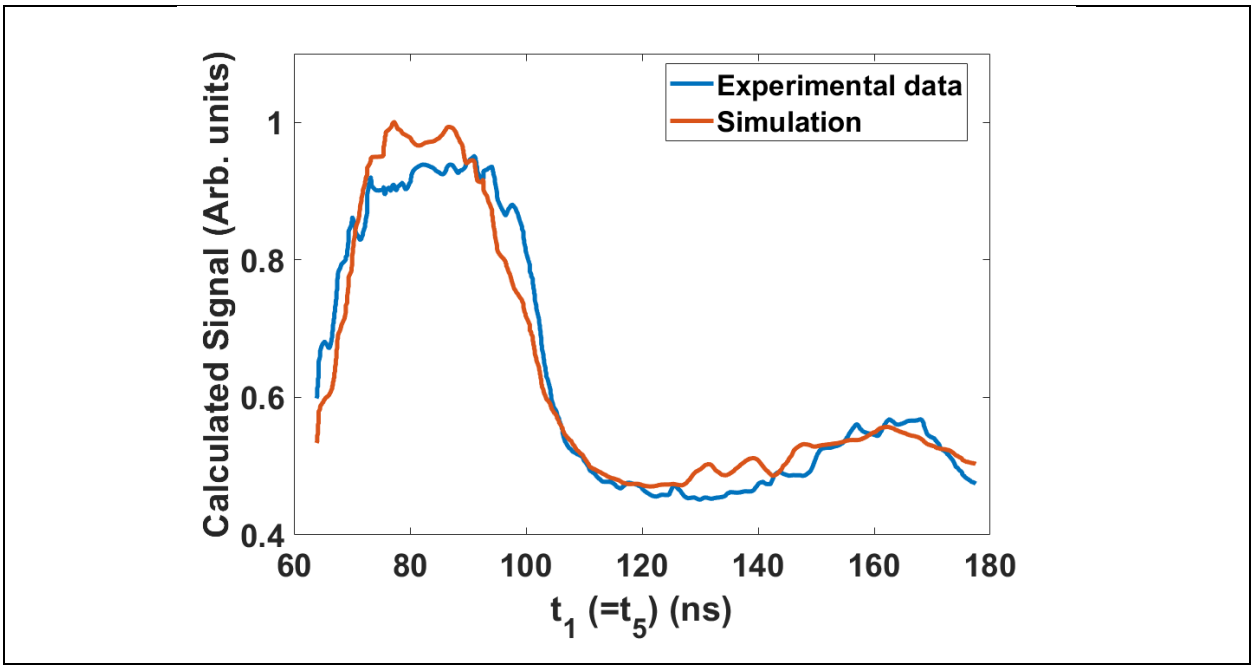

Fig. 11. The simulation made using the numerical algorithm of Sec. 4 to fit the experimental five-pulse DQM spectrum of the nitroxide biradical [20]. The experimental data shown is a profile of the three-dimensional experiment reported in [20], along the maximum slice at $t_5 = t_1$. The simulation parameters are: B_1 =17.8 G, *d=12.3 MHz*, $T_2^S = 500ns, T_2^D = 300ns$. The duration of the pulses is: $(t_p)_1 = (t_p)_3 = (t_p)_5 = 5ns$ and $(t_p)_2 = (t_p)_4 = 10ns$. The other parameters are listed in Table II. The simulation shows a reasonably good agreement with the experimental data, within experimental error.

Figures

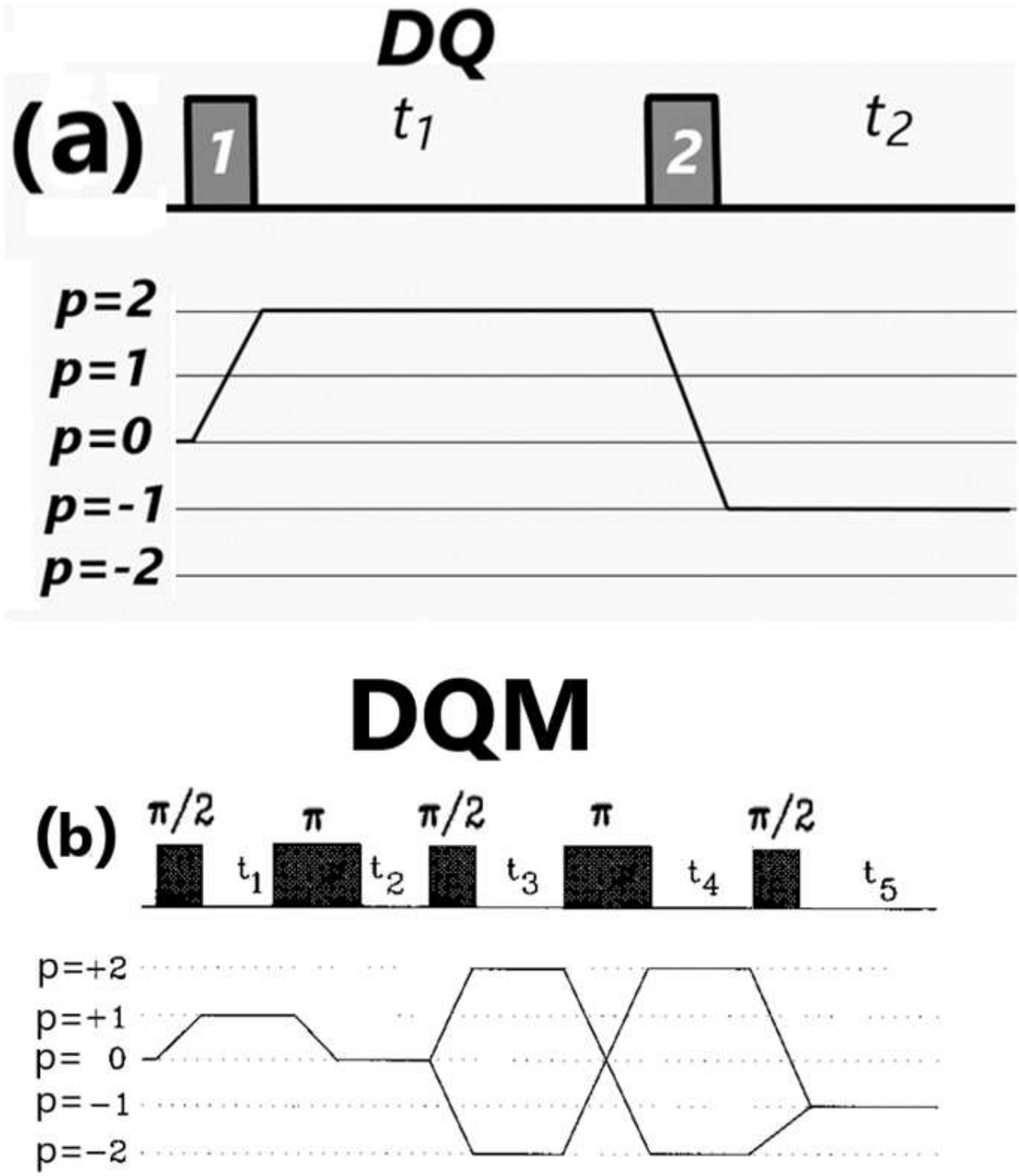

Figure 1

The pulse schemes and the relevant coherence pathways for (a) two-pulse DQ, where 1 and 2 are finite pulses of any duration; (b) five-pulse DQM. For the two-pulse DQ sequence, the tip angle is determined as β=γ_e B_1 t_p where B_1 is the amplitude of the microwave field and t_p is the duration of the pulse. For

five-pulse DQM, finite, with the tip angle being almost π/2, or π, are used as shown. Here p is the coherence order, which represents transverse magnetization, corresponding to the spins rotating in a plane perpendicular to the external field.

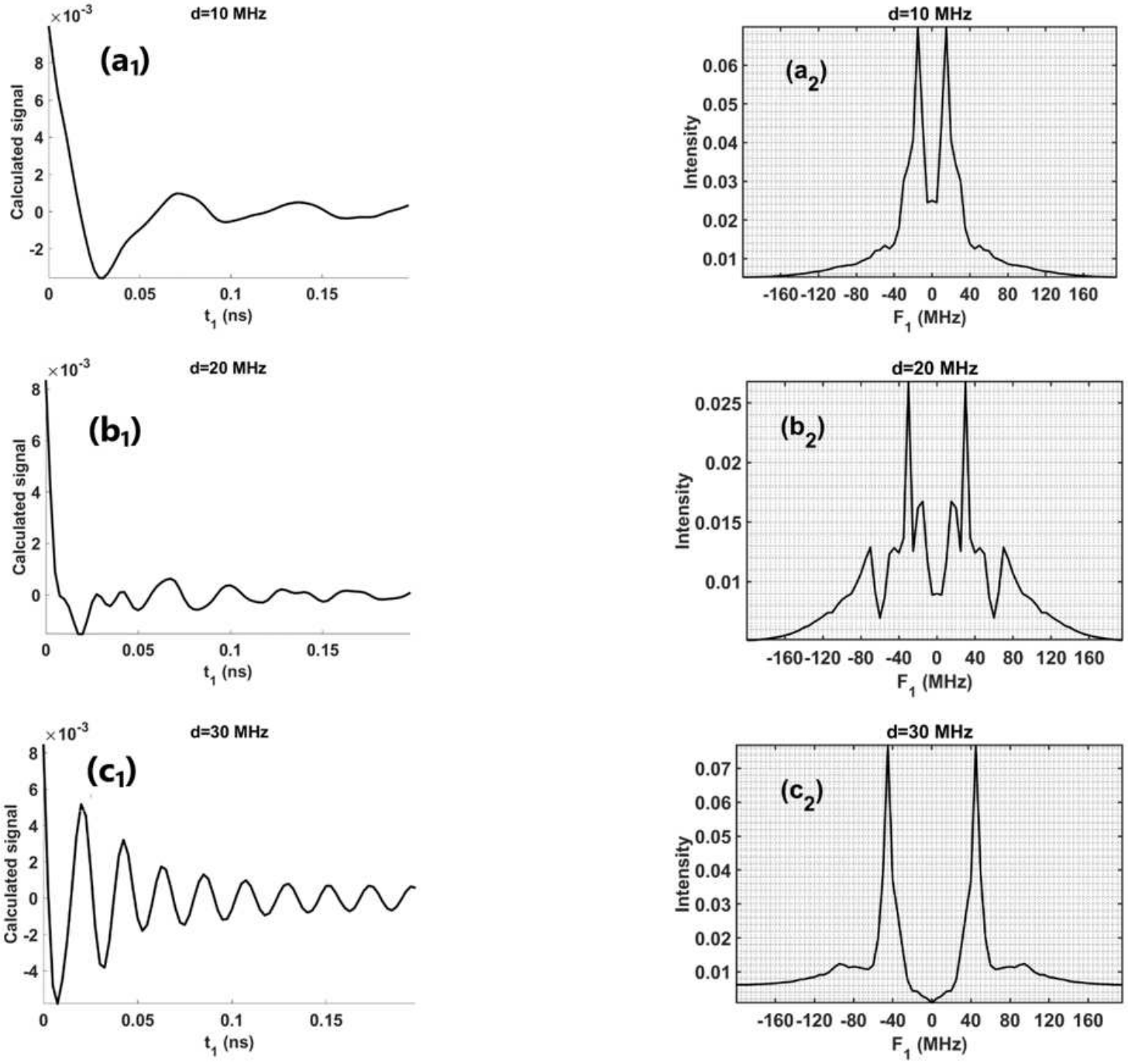

Figure 2

Dependence of the two-pulse DQ signal on dipolar-coupling constant for a polycrystalline sample, averaged over twenty Monte-Carlo orientations of the nitroxide dipoles: left (a_1,b_1,c_1) time domain DQ signals for t_2=2t_1 and right (a_2,b_2,c_2) their Fourier transforms (Pake doublets) for three different values of the dipolar-coupling constant d=10,20.30 MHz. The magnitude of the radiation microwave field

B_1=10G and the duration of the finite pulses t_p=80 ns are used for all simulations. All other parameters used for the simulations are listed in Table II. Relaxation is not considered in these simulations. All Pake doublets appear at ±3d/2, in agreement with those calculated analytically as given by Eq. (3.18).

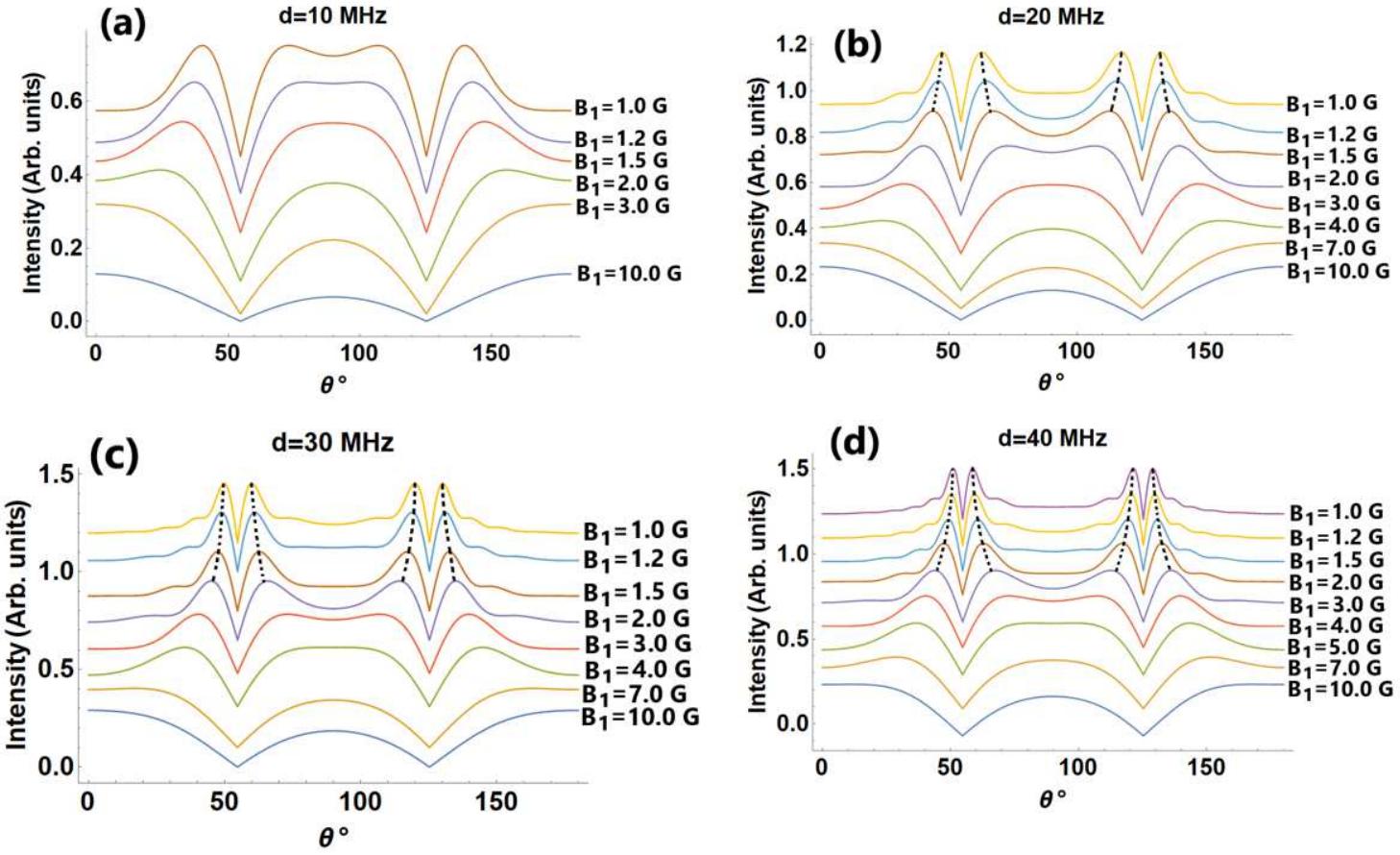

Figure 3

The coherence transfer T_0->2, as calculated using Eq. (3.12), plotted as function of θ for different values of the amplitude of the irradiation field, B_1, indicated next to each plot for (a) d=10 MHz, (b) d=20 MHz, (c) d=30 MHz and (d) d=40 MHz. The duration of the pulse t_p in each case is chosen consistent with a nominal π/2 pulse for each B_1 . Regardless of the values of d and B_1, the coherence transfer is zero at θ=54.74° and at θ=125.26°, i.e., the values which make (3cos^2 (θ)-1)=0. The orientational selectivity, related to the sharpness of the peaks, occurs at lower values of B_1 for each d value, as indicated by thick dotted lines in each figure. It is noted that there is no such value possible for d≤ 10 MHz.

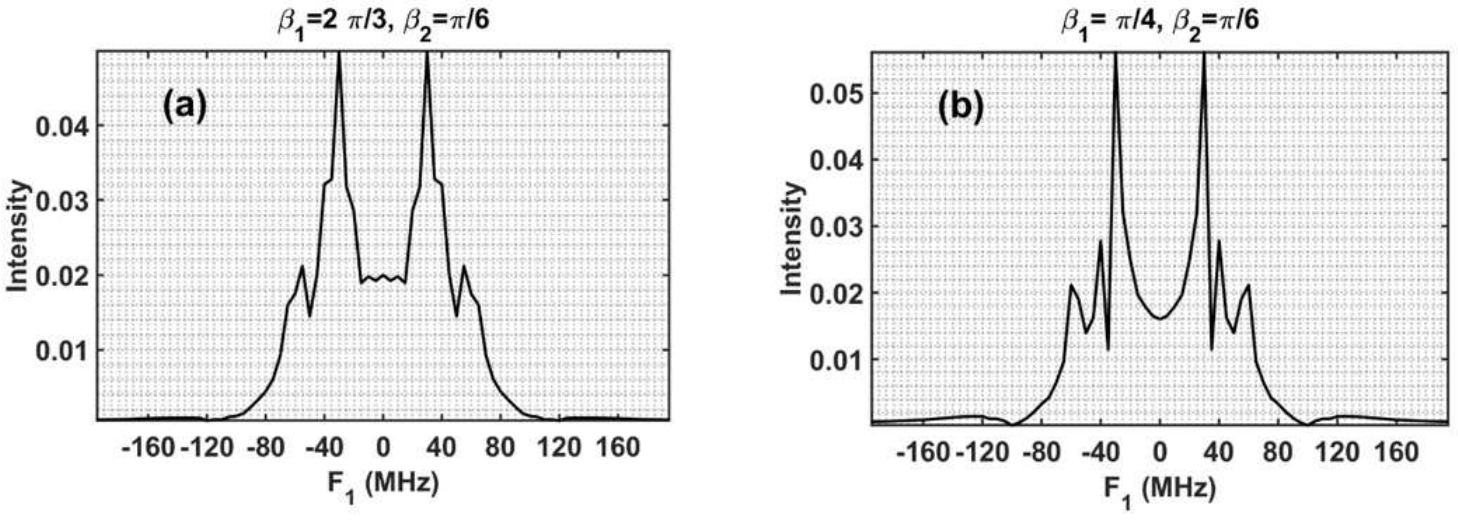

Figure 4

Orientational dependence of the two-pulse DQ signal. The effect of the orientation of the nitroxide radicals on the DQ Fourier transform for a polycrystalline sample is shown in this figure. The Fourier transform as a function of t_1 of the one-dimensional time-domain signal along t_2=2t_1 for the orientations of the two nitroxide dipoles: (a) (α_1,β_1,γ_1)=(0,2π/3,0),(α_2,β_2,γ_2)=(0,π/6,0) and (b) (α_1,β_1,γ_1)=(0,π/4,0),(α_2,β_2,γ_2)=(0,π/6,0). The dipolar coupling constant d=20 MHz and the amplitude of the irradiation microwave field B_1=10.0 G are used in the simulations. The values of all other parameters used in the simulations are listed in Table II. The Fourier transforms of the DQ signal are quite sensitive to the relative orientations of the nitroxide biradicals, making the DQ experiment feasible for structural studies.

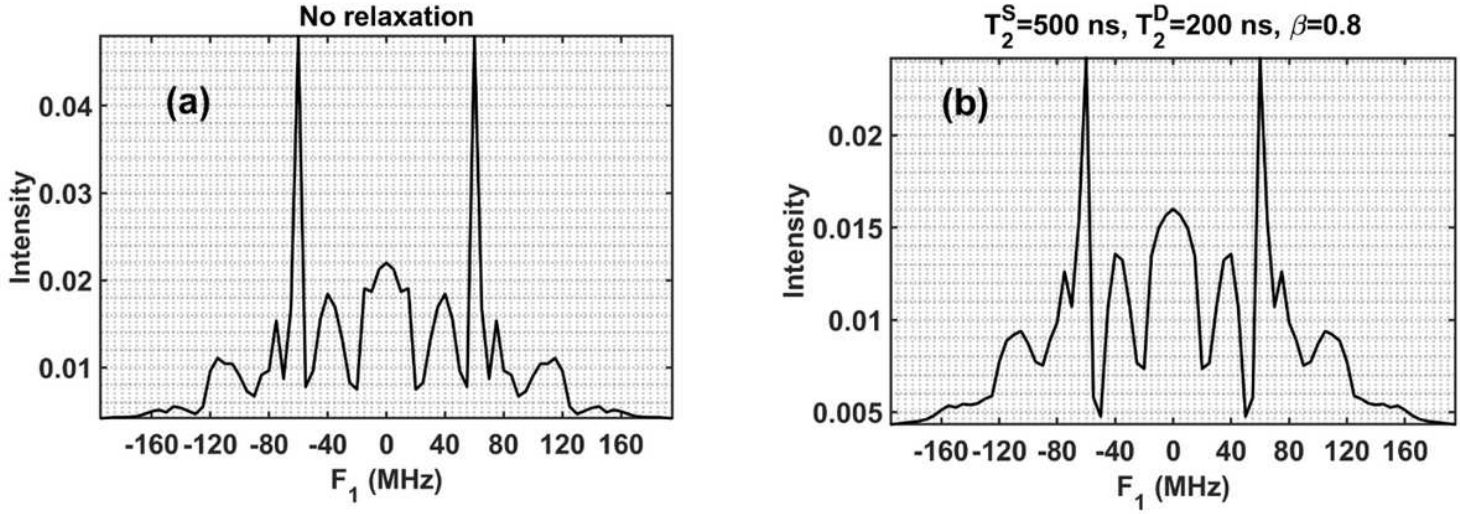

Figure 5

Effect of relaxation on the DQ signal for a polycrystalline sample, averaged over twenty Monte-Carlo orientations of the nitroxide dipoles. The Fourier transform as a function of t_1 of the time domain DQ signal at t_2=2t_1for: (left) without taking relaxation into account and (right) with relaxation included for

T_2^S=500 ns and T_2^D=200 ns using the stretching parameter β=0.8. The dipolar coupling constant d=40 MHz and the amplitude of the irradiation microwave field B_1=10.0 G are used in these simulations. The values of all the other parameters used in the simulations are listed in Table II. Due to relaxation, the peaks are broadened, and the intensity of the calculated Fourier transform of the DQ signal is reduced by a factor of two.

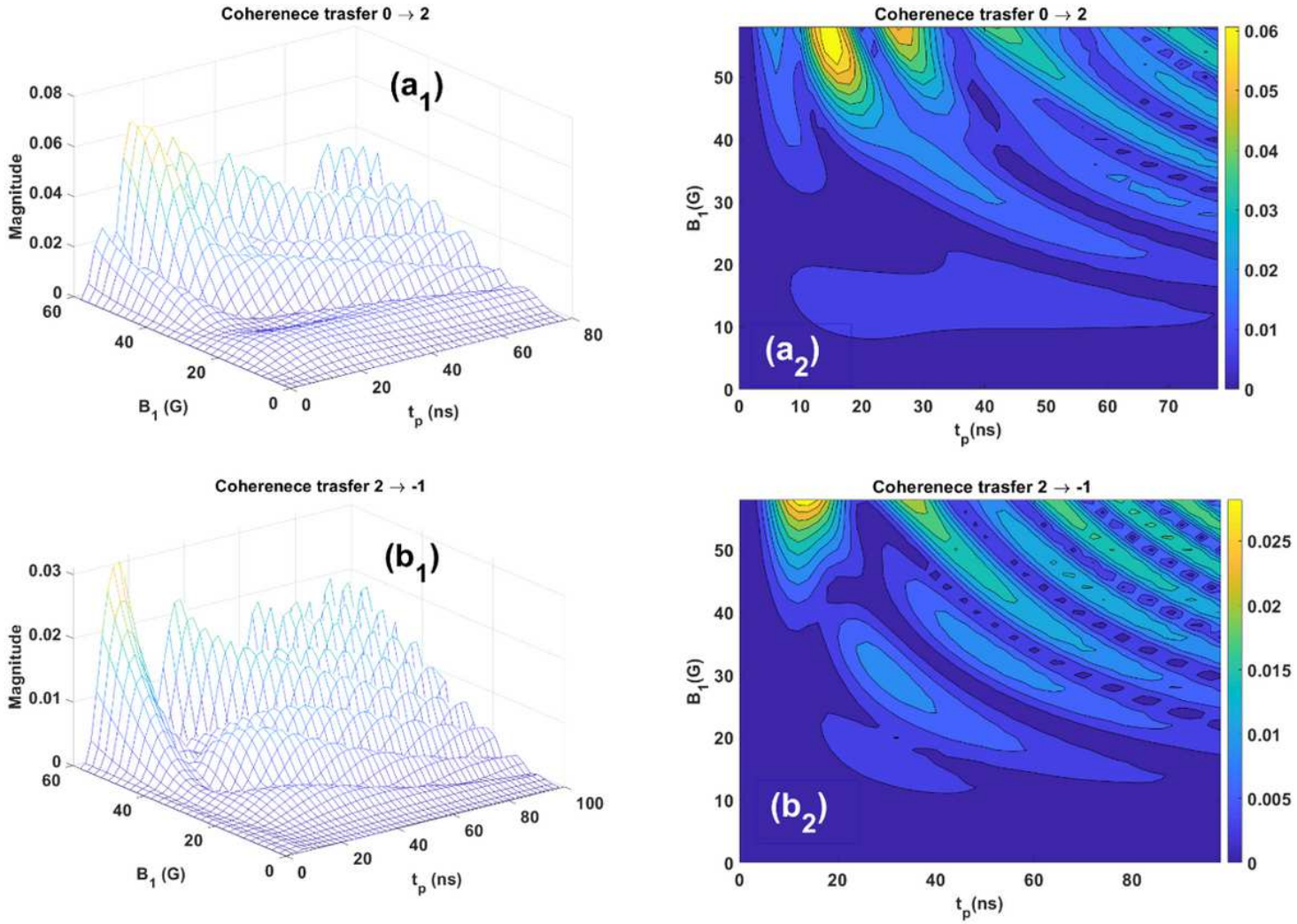

Figure 6

Two-pulse DQ coherence transfers for a polycrystalline sample, averaged over twenty Monte-Carlo orientations of the nitroxide dipoles: (left) absolute values and (right) their contour plots of (top) 0 -> 2 and (bottom) 2 ->-1 coherence transfers), as functions of the intensity of the microwave magnetic field B_1 and the duration of the pulses, t_p (the same duration was chosen for the two pulses) for the dipolar coupling constant d=10 MHz. All the parameters used for simulations are the same as those mentioned in the caption of Fig. 2. It is seen from these simulations that for the coherence transfers achieved with B_1=60 G and t_p=80 ns of ⍰0.10 or each of the T_0->2and T_(2->-1) transitions between the coherent pathways are reasonably large, making these B_1 and t_p values feasible for experimental purposes.

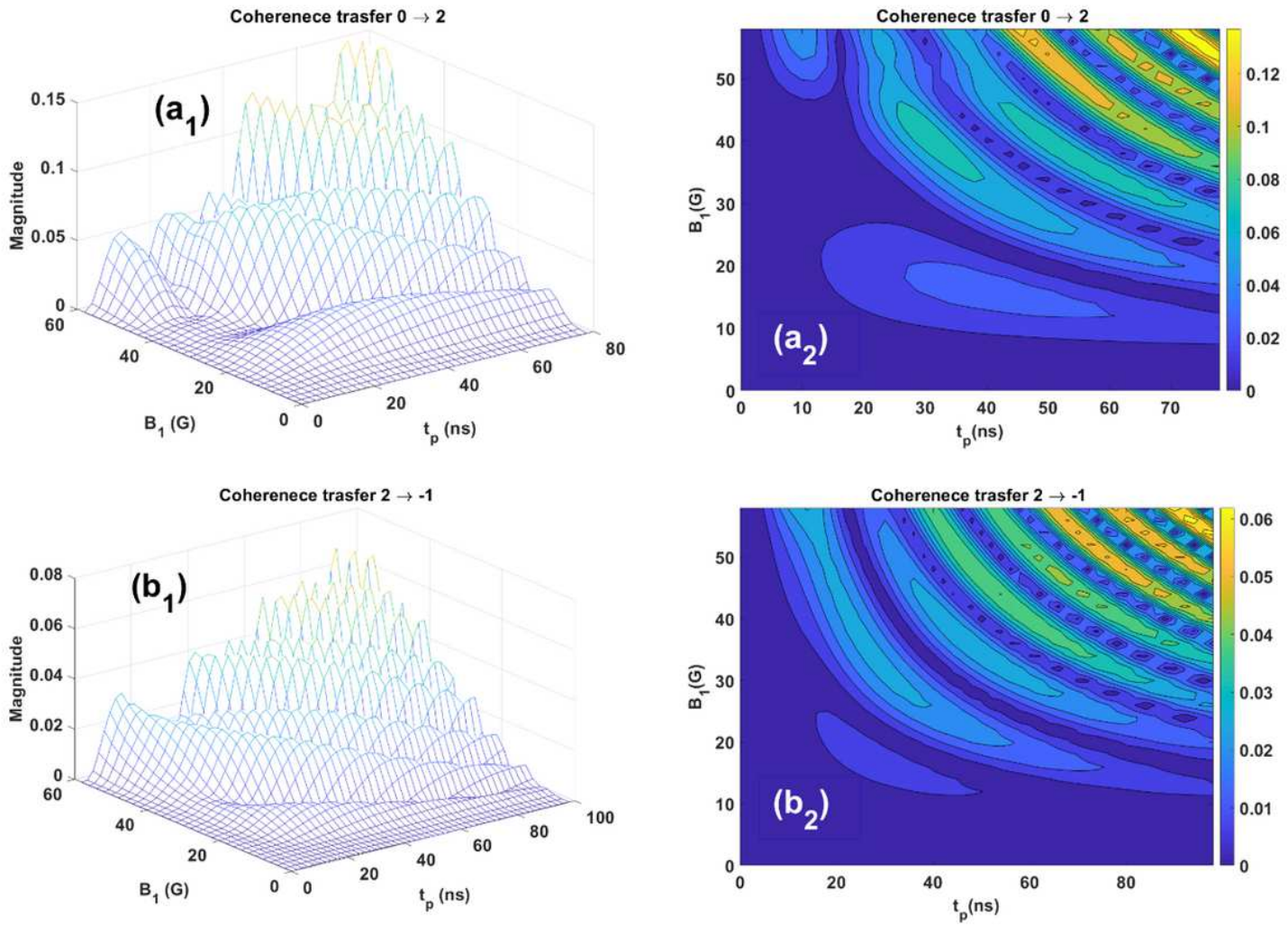

Figure 7

The same details as those for Fig. except that here the simulations are for the dipolar-coupling constant d = 30 MHz

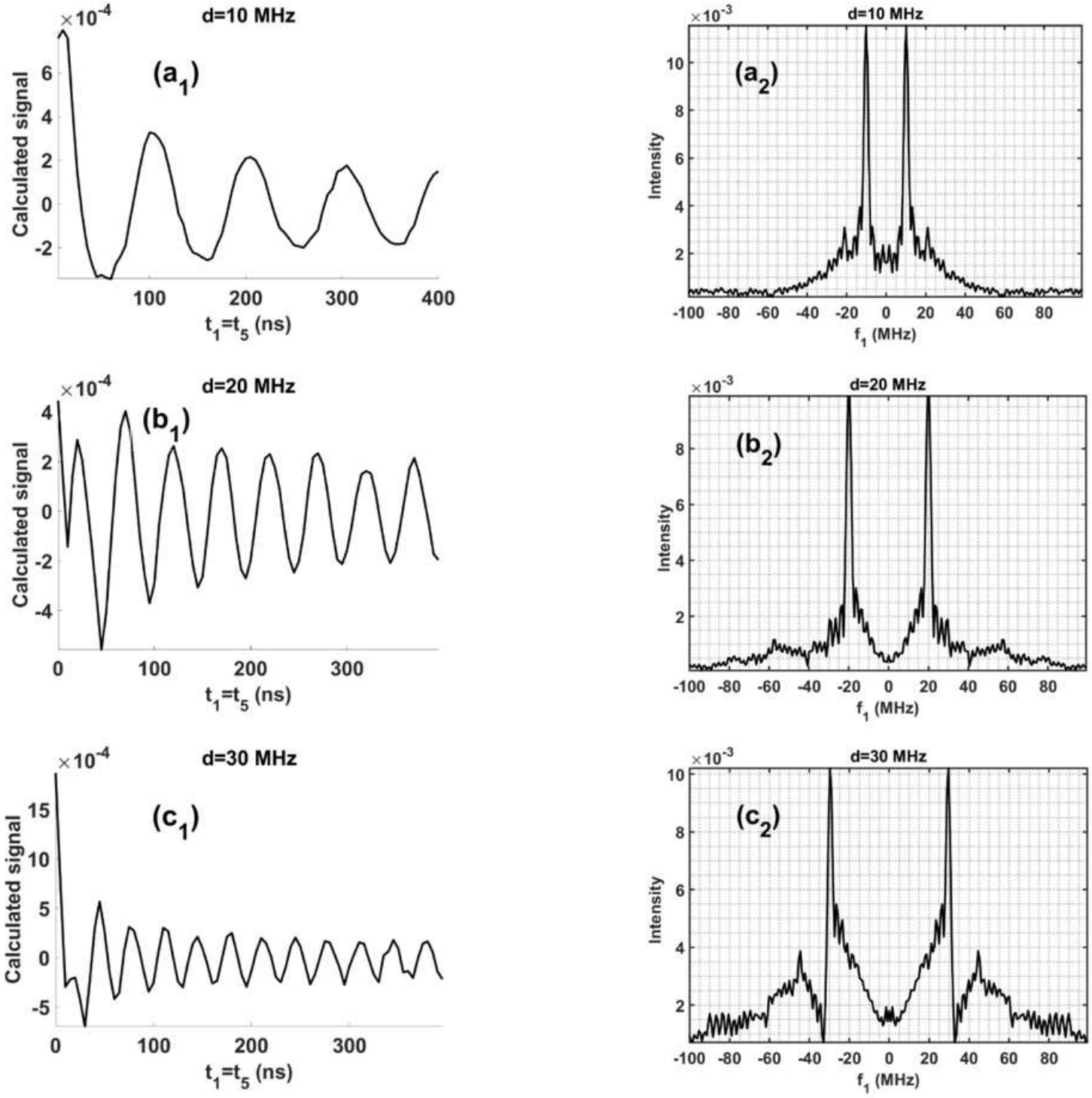

Figure 8

Dependence of the five-pulse DQM signal on dipolar-coupling constant for a polycrystalline sample, averaged over twenty Monte-Carlo orientations of the nitroxide dipoles: left (a_1,b_1,c_1) time domain DQ signals for t_5=t_1 and right (a_2,b_2,c_2) their Fourier transforms (Pake doublets) for three different values of the dipolar-coupling constant d=10,20.30 MHz. The magnitude of the radiation microwave field B_1=17.8G and the duration of the finite pulses (t_p)_1=(t_p)_3=(t_p)_5=5ns and (t_p)_2=(t_p)_4=10ns ns are used for all simulations. All other parameters used for the simulations are listed in Table II.

Relaxation is not considered in these simulations. All Pake doublets appear at ±d, in agreement with those calculated analytically as given by Eq. (3.20).

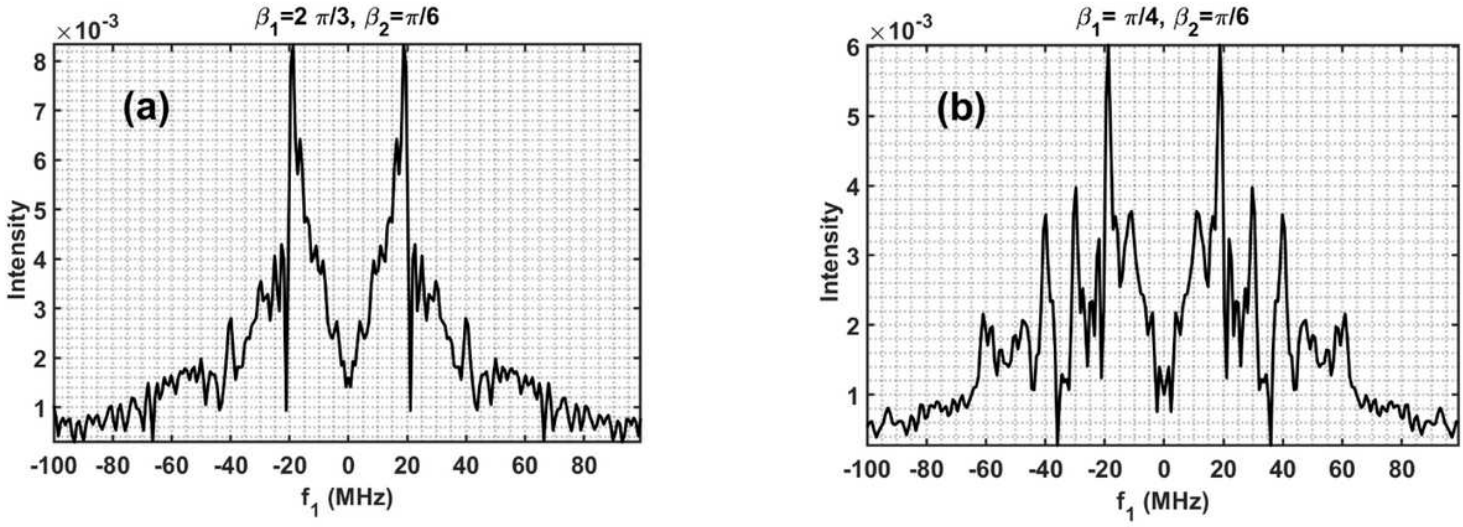

Figure 9

Orientational dependence of the five-pulse DQM signal. The effect of the orientation of the nitroxide radicals on the DQM Fourier transform for a polycrystalline sample is shown in this figure. The Fourier transform as a function of t_1 of the one-dimensional time-domain signal along t_2=2t_1 for the orientations of the two nitroxide dipoles: (a) (α_1,β_1,γ_1)=(0,2π/3,0),(α_2,β_2,γ_2)=(0,π/6,0) and (b) (α_1,β_1,γ_1)=(0,π/4,0),(α_2,β_2,γ_2)=(0,π/6,0). The dipolar coupling constant d=20 MHz and the amplitude of the irradiation microwave field B_1=17.8 G are used in the simulations. The values of all other parameters used in the simulations are listed in Table II. A comparison of Figs. (a) and (b) shows that the Fourier transforms of the DQM signal are quite sensitive to the relative orientations of the nitroxide biradicals, making the DQM experiment feasible for structural studies.

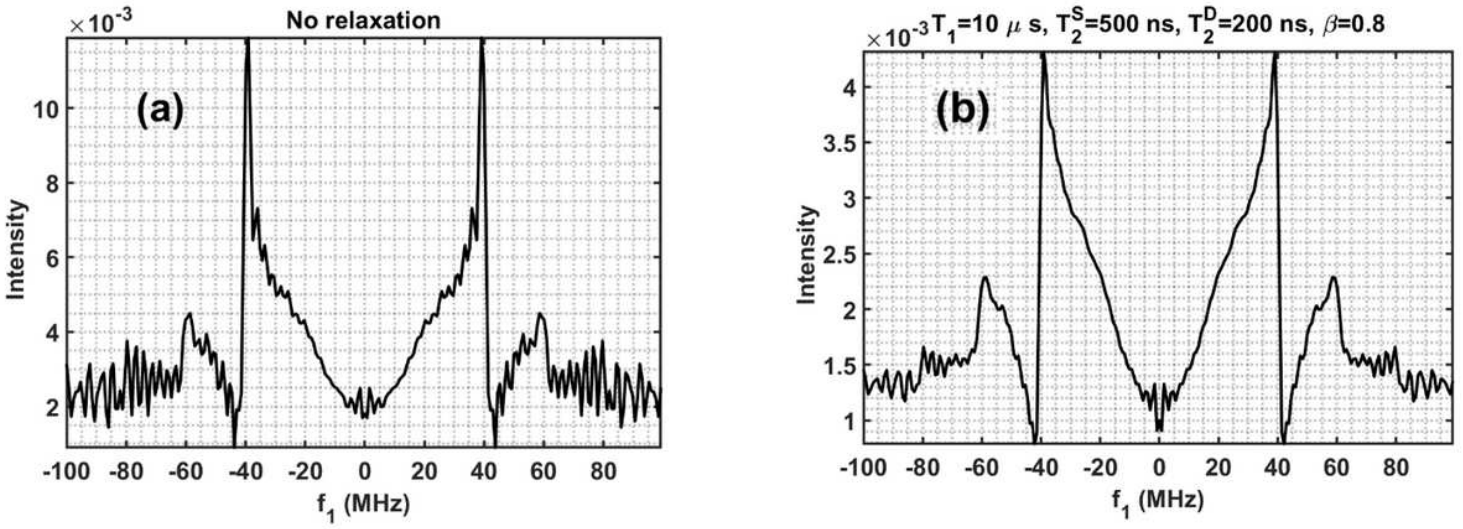

Figure 10

Effect of relaxation on the DQM signal for a polycrystalline sample, averaged over twenty Monte-Carlo orientations of the nitroxide dipoles. The Fourier transform as a function of t_1of the time domain DQM signal at t_5=t_1for: (left) without taking relaxation into account and (right) with relaxation included for T_2^S=500 ns and T_2^D=200 ns using the stretching parameter β=0.8. The dipolar coupling constant d=40 MHz and the amplitude of the irradiation microwave field B_1=17.8 G are used in these simulations. The values of all the other parameters used in the simulations are listed in Table II. Due to relaxation, the peaks are broadened, and the intensity of the calculated Fourier transform of the DQM signal is reduced by a factor of three.

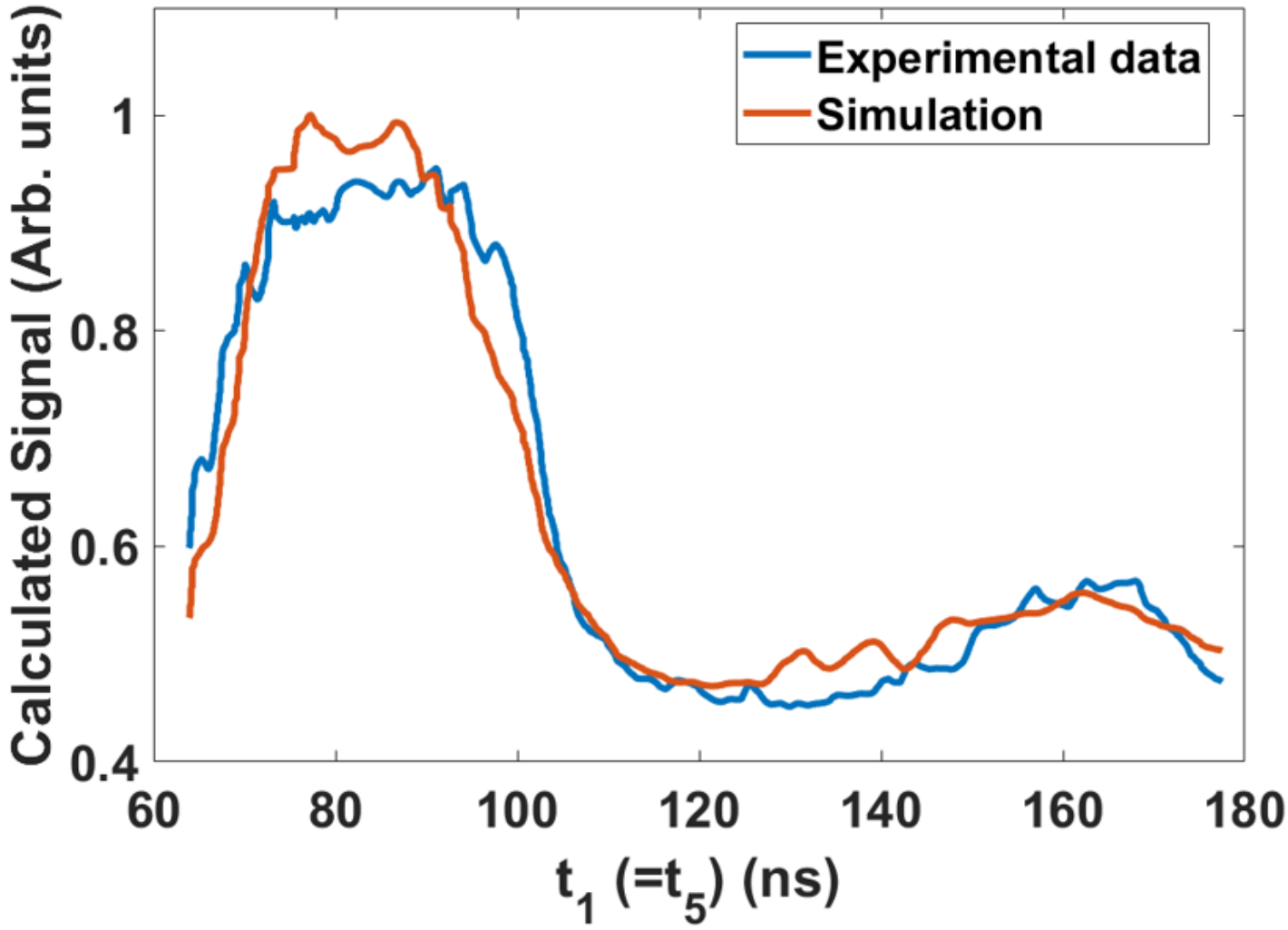

Figure 11

The simulation made using the numerical algorithm of Sec. 4 to fit the experimental five-pulse DQM spectrum of the nitroxide biradical [20]. The experimental data shown is a profile of the three-dimensional experiment reported in [20], along the maximum slice at t_5=t_1. The simulation parameters are: B_1=17.8 G, d=12.3 MHz, T_2^S=500ns, T_2^D=300ns. The duration of the pulses is: (t_p)_1=(t_p)_3= (t_p)_5=5ns and (t_p)_2=(t_p)_4=10ns . The other parameters are listed in Table II. The simulation shows a reasonably good agreement with the experimental data, within experimental error.

Supplementary Files

This is a list of supplementary files associated with this preprint. Click to download.

- SupFile2pulseDQ5pulseDQM15Feb21.docx